# PERFORMANCE OF RECALIBRATION SYSTEMS OF GCM FORECASTS OVER SOUTHERN AFRICA

by

**Mxolisi Excellent Shongwe**

Submitted in partial fulfillment of the requirements
for the degree

## MASTER OF SCIENCE

in the

Faculty of Natural and Agricultural Sciences
University of Pretoria

July 2006

# PERFORMANCE OF RECALIBRATION SYSTEMS OF GCM FORECASTS OVER SOUTHERN AFRICA

**Mxolisi Excellent Shongwe**

Promoter: Prof. Willem A. Landman
Department: Department of Meteorology
Faculty: Faculty of Natural and Agricultural Sciences
University: University of Pretoria
Degree: Doctor of Philosophy

**SUMMARY**

This study assesses the performance of an atmospheric GCM forced with persisted SSTs in simulating austral summer precipitation at smaller spatial (regional) scales. Two statistical recalibration techniques of differing technical complexity are then presented and compared to get an idea as to which method among them is best suitable for southern Africa. The two regression-based methods applied in recalibrating the ECHAM4.5 GCM output during austral summer in southern Africa are based on model output statistics (MOS) using principal components regression (PCR) and canonical correlation analysis (CCA) to statistically link archived records of the GCM to regional rainfall over much of Africa south of the equator. A linear statistical model linking near-global sea-surface temperatures (SSTs) to regional rainfall is also developed.

Southern Africa is divided into 18 homogeneous regions using cluster analysis. The potential predictive skill of summer precipitation over each region from raw-GCM ensembles, the linear statistical and MOS models is evaluated using the relative operating characteristics (ROC) score and the ranked probability skill score computed over a 12-year retroactive period 1989/90–2000/01..

The MOS technique outperforms the raw GCM ensembles and the linear statistical model in certain cases. On many occasions, the PCR-MOS performs better than CCA-MOS but the former does not show clear superiority over the latter method because the two methods are in a broad sense performing the same task. The need to recalibrate GCM predictions at regional scales to improve their skill at smaller spatial scales is demonstrated in this study.

## ACKNOWLEDGEMENTS


- It is by the grace of the Almighty God that I have been able to undertake this MSc research. I give thanks first and foremost to the Lord for His mercies that endure forever. I want to return praise to Him for providing me the opportunity to do a Masters Degree so shortly after completing a BSc degree. According to scriptures: 'A man can receive nothing, except it be given him from heaven' (John 3:27). I acknowledge with gratitude the Lord's mercy, favour and Divine backup in my life as evidenced by the success I am continually enjoying in my career; "It is not him that willeth, nor him that runneth, but God that sheweth mercy" (Rom. 9:16), and "Every good gift and every perfect gift is from above, and cometh down from the Father of lights, with whom is no variableness, neither shadow of turning" (Jam. 1:17). Blessed be the name of God forever and ever: for wisdom and might are His: and He changeth the times and the seasons: He removeth kings, and setteth up kings: He giveth wisdom unto the wise, and knowledge to them that know understanding (Dan. 2:20-21).
- I would like to express my sincere thanks and appreciation to my supervisor Prof. Willem A. Landman for soliciting funding, and also for his guidance, motivational support, and his thoughtful and constructive comments and suggestions during the course of this work.
- Dr. Simon Mason helped with designing the Climate Predictability Tool (CPT), software which has been used in this research to perform the Principal Components Regression and Canonical Correlation Analysis. He has also been very helpful in calculating the skill scores by designing the Relative Operating Characteristics (ROC) tool. In addition Drs. Mason and Matayo Indeje were helpful in providing some useful reference material.
- Special thanks are expressed to Emily Grover-Kopec for helping in extracting the GCM and SST data from the International Research Institute for Climate Prediction (IRI) Data Library.
- Anna Bartman from the South African Weather Service is thanked for her help in delineating the homogeneous rainfall regions, and Estelle Marx made some of the maps.
- The Southern African Development Community (SADC) Drought Monitoring Centre, Harare (DMC-H) provided the station rainfall data used in this research.
- I also extend my gratitude to the Director of the Swaziland National Meteorological Service for allowing a flexible working environment.

# TABLE OF CONTENTS

## LIST OF FIGURES

## LIST OF TABLES

# 1.0 CHAPTER 1 INTRODUCTION

## *1.1 Background*

The irregular recurrence of anomalous climate events such as droughts and floods demonstrate an urgent need for the enhancement of accurate seasonal to inter-annual climate monitoring and prediction in the Southern African Development Community (SADC) region. Most of the national economies within the region are highly dependent on agriculture and water resources hence are vulnerable to year-to-year fluctuations in the amount and distribution of precipitation. Following the 1991-92 El Niño-related drought, and its adverse effects over many parts of the globe including the SADC region, understanding and techniques behind climate forecasting have rapidly evolved during the most recent decade (Hastenrath et al. 1995; Barnston et al. 1996; Mason et al. 1996; Makarau and Jury 1997; Rocha and Simmonds 1997b; Mason 1998; Tennant 1999; Landman and Mason 1999; Landman and Tennant 2000; Landman et al. 2001; Unganai and Mason 2002; Landman and Goddard 2002). The progress being made in exploring prospects for seasonal climate prediction over the region using techniques of varying complexity is encouraging.

Earlier approaches to climate forecasting involved the use of purely statistical methods such as multiple linear regression (Mason et al. 1996; Makarau and Jury 1997), discriminant analysis (Mason 1998), canonical correlation analysis (Barnston et al. 1996; Landman and Mason 1999b), and neural networks (Hastenrath et al. 1995). Statistical climate forecasting techniques rely on empirical relationships between climate variables to give an indication of the expected regional climate anomalies based on prevailing larger-scale climate anomaly patterns. Their success is therefore dependent on the amount and quality of available historical data. Observational surface data is available for much of SADC save for a few countries that have been victims of civil wars and political volatility, creating prospects for successful application of statistical tools in seasonal climate forecasting. Statistical methods, particularly those that are linear, are often preferred because they are relatively simple and cheaper to develop. However the predictive skills of these models are limited owing to the exclusion of non-linear

relationships amongst variables. Statistical methods are trained using historical data such that past outcomes are averaged with an inherent inability to distinguish one situation from generic events (e.g. forcing from anomalous warming (cooling) in the eastern equatorial Pacific Ocean would often yield predictions of below- (above-) average rainfall over southeastern SADC). However, linear relationships amongst climate variables have been found not to be always stable (Landman and Mason 1999a). Linear statistical models are unable to account for such instabilities in the link amongst climate variables. In a MOS setup such instabilities in the relationship amongst climate variables are at least quantitatively simulated by the GCM simulations. Furthermore, most statistical methods inherently assume multivariate normality among the populations of the variables, an assumption that may be invalid.

Noting that much of the potential of statistical models has already been realised, development efforts are now shifting towards more sophisticated numerical models that represent the physics of the climate system. Theoretically, dynamical models of the climate system offer a possible solution to the severe deficiencies of statistical models. Since general circulation models are based on the first principles of the processes governing the climate system, with improved and more detailed representation of the real physics, there is room for further improvement in forecast skill. General circulation models have demonstrated skill in simulating large-scale atmospheric features (Joubert 1997), but are not equally skilful at much smaller spatial scales. The perceived failure of climate models on the local scale can be attributed to their coarse horizontal resolution whereby the structure of the earth's surface is not adequately described in the models. Consequently, subgrid-scale processes such as those related to topography and land-water distribution, which strongly influence regional precipitation thus shaping regional or local climates, are not explicitly resolved by the models. The use of spatially uniform parameterisation schemes for different locations in the world could produce additional errors in GCM simulations. Unfortunately, for most climate forecast applications such as in agriculture, water resources, and energy and transport systems, it is subgrid scale information that is useful. There is therefore a need to bridge the spatial mismatch

through some form of recalibration of GCM output by relating large-scale information from climate models to regional or local climate parameters.

The derivation of smaller scale information from low-resolution GCMs through some form of transformation is generally referred to as downscaling or recalibration. Downscaling is normally based on the link between large-scale GCM-simulated atmospheric fields and local climate parameters such as station rainfall. The downscaling methods found in literature vary in their technical complexity. Dynamical downscaling approaches involve using a much finer GCM resolutions up to T106 (about 1.125º) or nesting a limited area model (LAM) within a GCM (Giorgi 1990; Giorgi et al. 1994; Kidson and Thompson 1998; Murphy 1999, 2000). However, both methods are computationally intensive and most expensive hence restricted to institutions with sufficient computational power. A less computer intensive and cheap approach is statistical downscaling whereby relationships between GCM simulated large-scale circulation and regional rainfall is derived empirically. Almost all statistical recalibration methods establish a statistical model based on empirical relationships between archived large-scale GCM-simulated atmospheric fields and regional rainfall, which is then applied in translating the GCM information into smaller spatial scales consistent with user requirements. In certain cases however, such as in numerical weather prediction, the method of perfect prognosis (Wilks 1995; Landman et al. 2001) is used. In this technique, it is observed large-scale atmospheric fields that are statistically linked to observed regional climate, and the derived relationships later applied to GCM-simulated fields. Several statistical downscaling techniques of varying complexity are being applied. Zorita and von Storch (1999) give a review of some of the statistical methods in use.

In this study, two regression-based recalibration methods are applied and the operational levels of their forecast skill are assessed using a retroactive forecast procedure (Landman et al. 2001). The methods considered are canonical correlation analysis (CCA) and principal components regression (PCR). The method of PCR, whose procedure is simpler, has been previously used in atmospheric sciences for downscaling coarsely gridded climate data from GCMs to a finer spatial resolution (Mo and Stratus, 2002) but not nearly extensively as CCA, which has also been used to recalibrate GCM output to

specifically defined rainfall regions (Karl et al. 1990; von Storch et al. 1993; Zorita and von Storch 1999; Landman and Tennant 2000; Busuioc et al. 1999, 2001; Landman and Goddard 2002, 2005). The performance of the recalibration systems is further compared with that of raw GCM ensembles and a simple linear statistical model. These forecasting models provide a baseline of skill for the recalibration methods that is more difficult to beat than much simpler forecasting schemes such as persistence.

### *1.2 Climatology of Southern Africa*

Southern Africa is used in the context of this report to refer to contiguous SADC. The present study is limited by historical data availability to 11 countries within SADC. The countries whose observational station data are used are shown in Figure 1.

Over the SADC region, amongst other space-time varying climate parameters, precipitation exhibits the highest degree of spatial and temporal variability. Figure 2 (top map) shows the mean annual rainfall over the region based on the 1961–2000 period. Notably, precipitation generally increases from southwest to northeast. The western coast of the region bordering the cold Benguela current, which includes northwestern South Africa and southern Namibia, receives annual total rainfall less than 200 mm on average. Further inland, amounts increase gradually to reach about 500 mm or less over the extensively flat region, which include Botswana, northern Namibia and much of western South Africa. Despite receiving rainfall amounts up to 500 mm, these semi-arid areas, which encompass the Kalahari and Namib deserts, are generally the driest in the region from a climatological perspective. Over the eastern parts of South Africa, partly in response to orographic forcing, rainfall distribution is uneven, with only localised rainfall maxima exceeding 1000 mm over Lesotho and the Drakensberg mountains of South Africa (Taljaard 1996), and even over northeastern South Africa. Along the southeastern coast, partly in response to the warm currents, rainfall in excess of 900 mm is received. Rainfall amounts increase further north closer to the mean surface position of the ITCZ (about 15ºS) during summer. Local features still play a significant role in forcing an uneven rainfall spatial distribution. Rainfall maxima exceeding 1000 mm occur over the seaward side of the Chimanimani and Inyanga mountains, along the eastern border of

Zimbabwe extending into central Mozambique. Further north, a large area extending from central Zambia, Malawi and southern Tanzania receive more than 900 mm of rainfall. The highlands of southern Tanzania receive much higher amounts, more than 1200 mm per annum.

Much of SADC experiences one major rainfall season centred on December-January-February associated with the extreme southward position of the Inter-Tropical Convergence Zone (ITCZ). During this season precipitation is predominantly convective. The spatial distribution of the long-term mean of summer precipitation amounts, which shows a similar pattern to the mean annual pattern, is shown in Figure 2, bottom left. But it is more informative to express these amounts as a percentage of the annual total as shown in Figure 2, bottom right. It is evident from the figure that an extensive area within the region receives more than 80 per cent of the annual total during austral summer. This typifies areas whose rain-bearing systems are mainly of tropical origin. When considering such a large domain exceptions inevitably occur. For instance, most equatorial stations south of the equator and some parts of the Benguela coast receive less than 65 per cent of their annual total during austral summer. These areas experience a bimodal rainfall distribution with peaks around October-December and March–May (Mutai et al. 1998; Indeje 2000). The annual rainfall cycle representative of such region is shown in Figure 3(c). The two rainfall peaks occur as the ITCZ passes through these areas in its seasonal migration twice every calendar year. The southwestern coast (region 2; Figure 1) is exposed to midlatitude systems and is an austral winter rainfall area. This area receives less than 35 per cent of its total annual rainfall during austral summer. The corresponding annual cycle, which shows a clear winter maximum, is shown in Figure 3a. The southern coast of South Africa (region 2; Figure 1) receives rainfall all-year-round with maxima during transition seasons. The annual march of rainfall in this region is shown in Figure 3b.

The rainfall patterns over much of the SADC region is influenced by several large-scale systems including: the ITCZ, anticyclones and associated ridging systems, lows and depressions and associated trough systems, semi-stationary and travelling waves, wave

interactions between low- and middle-latitude flow, and jet streams, amongst others. The effect of these systems is modified at regional and local scales by several surface characteristics; some of these are discussed in the sections that follow. The surface features play a crucial role mainly in determining the weather pattern at shorter time-scales. At seasonal to interannual time-scales other factors play an important influential role. They include: teleconnections with global climate anomalies such as those associated with sea-surface temperatures, the quasi-biennial oscillation (QBO) in the lower stratospheric zonal wind, and solar activities, amongst others. Tyson and Preston-Whyte (2000) devoted considerable attention to large-scale weather-producing processes and systems over southern Africa, as well as to teleconnection patterns influencing the regional climate. In this report, some of these systems and patterns, and their influential role on the climate of the region will be discussed.

Of the weather-producing large-scale systems, the seasonal migration of the ITCZ plays a leading role in determining the rainfall pattern over the bulk of the SADC region. The seasonal migration of the ITCZ follows that of the overhead sun, to be located about 17ºS in southern midsummer (Taljaard 1984). The ITCZ creates a favourable environment for pronounced convective activity resulting in unsettled and often rainy weather in its vicinity. Over southern Africa, during its southernmost position, the ITCZ is associated with several convergence zones of airstreams from the southwest Atlantic (the St. Helena anticyclone), the cross-equatorial monsoonal flow from the north-east, and the deep tropical easterlies from the Indian Ocean (Tyson and Preston-Whyte 2000). A thermal low typically develops over the central interior, preferentially over Botswana, associated with the ITCZ. Deep moist easterly flow originating from the southwest Indian Ocean penetrates the subregion recurving southward towards the thermal trough. This scenario is favourable for the development of a widespread cloud band and convective precipitation usually oriented in an approximately north-south axis due to the link between southward moving tropical air and midlatitude depressions to the south of the sub-continent. The tropical-temperate troughs arising from this link are one of the major ITCZ-related rain-producing systems over southern Africa.

Over southern Africa, the intra- and interseasonal variations in location and intensity of two semi-permanent anticyclones associated with the sub-tropical high pressure belt dominate the circulation, particularly at lower levels. The anticyclones form adjacent to the subcontinent over southeast Atlantic (the St. Helena high) and southwest Indian Oceans (the Mascarene high). They are centred about 28ºS and 33ºS in winter and summer, respectively.

The southern African countries experience either a direct or indirect influence from tropical depressions/cyclones, which form over the southwest Indian Ocean during late summer. Anomalously warm SSTs over this part of the ocean in summer create favourable conditions for the formation of these disturbances.

### *1.3 Factors influencing the climate and its variability*

Southern African climate responds to several forcing mechanisms, external and direct regional or local forcing, as well as large-scale atmospheric influences from remote locations. A number of studies have provided evidence on the influence that several control systems and factors, remote and nearby, exert on tropical and southern African atmosphere, and a theoretical basis for understanding the mechanisms underlying the linkage (e.g. Asnani 1993; Taljaard 1994; Tyson and Preston Whyte 2000). In this section an attempt is made to list and discuss some factors, which are believed to underlie the marked spatio-temporal weather hence climate variability over the region. Some teleconnection patterns have been found to play a crucial role in determining seasonal to interannual climate variability in the region, and will be discussed.

Several surface characteristics of the region play a major role in influencing the climate dynamics. Of the known lower boundary factors forcing strong atmospheric response regionally and locally, distribution of land and sea, and orography play a significant role in determining the long-term rainfall pattern. The subcontinent is bordering the Indian Ocean to the east and the Atlantic to the west. The forcing from these oceans modulates the regional climate and they are the major source regions of maritime airmasses affecting the subregion at shorter timescales. Of specific importance for southern African

climate are the contrasting ocean currents on the east and west coasts. The existence of the warm currents (i.e. the Agulhas and the train of mesoscale eddies moving polewards along the Mozambique channel (Reason et al. 2006)) along the east coast and cold currents (the Benguela system), and coastal upwelling along the western coast is partly responsible for the observed southwest to northeast gradient in the long-term mean rainfall pattern.

Figure 4 shows a detailed map of the topography of the SADC region, which plays a significant role in distorting the effect of large-scale circulation at regional or smaller scales within the region. It is evident from the map that much of inland SADC is a moderately elevated plateau reaching heights more than 1000 m above mean-sea-level over a large part, but with heights greater than 1500 m above mean-sea-level over an extensive area. Noteworthy areas with high ground, reaching more than 2000 m above mean-sea-level are eastern South Africa, and Lesotho. Over eastern Democratic Republic of Congo, mountains extending up to more than 2000 m are found, as well as along the area from Lake Tanganyika extending southwards into Malawi. The existence of mountain ranges modulates the climate by inducing orographic convective precipitation systems, influencing the development and maintenance of meso-scale circulations, and the blocking and channelling effects on the low-level air streams (Indeje 2000). Typical examples where surface features such as orography distort the large-scale circulation and benefit localised areas are over northeastern South Africa where these features result in highest mean annual rainfall over an isolated station such as Malelane, and the eastern border of Zimbabwe where highest amounts of rainfall are received in response to forcing from the Chimanimani and Inyanga mountains. Taljaard (1994) give a detailed discussion of the topography of southern Africa and its effect on the precipitation pattern.

Another surface feature, which modifies the effect of large-scale circulation at smaller spatial scales, is the presence of inland large water bodies such as Lake Victoria over northwestern Tanzania, Lake Tanganyika on the western Tanzanian border and Lake Malawi. These forcing features are respectively ranked second, seventh and tenth in the world in terms of areal coverage, and they influence local climates through diurnal meso-scale circulations in the form of land/lake breeze systems.

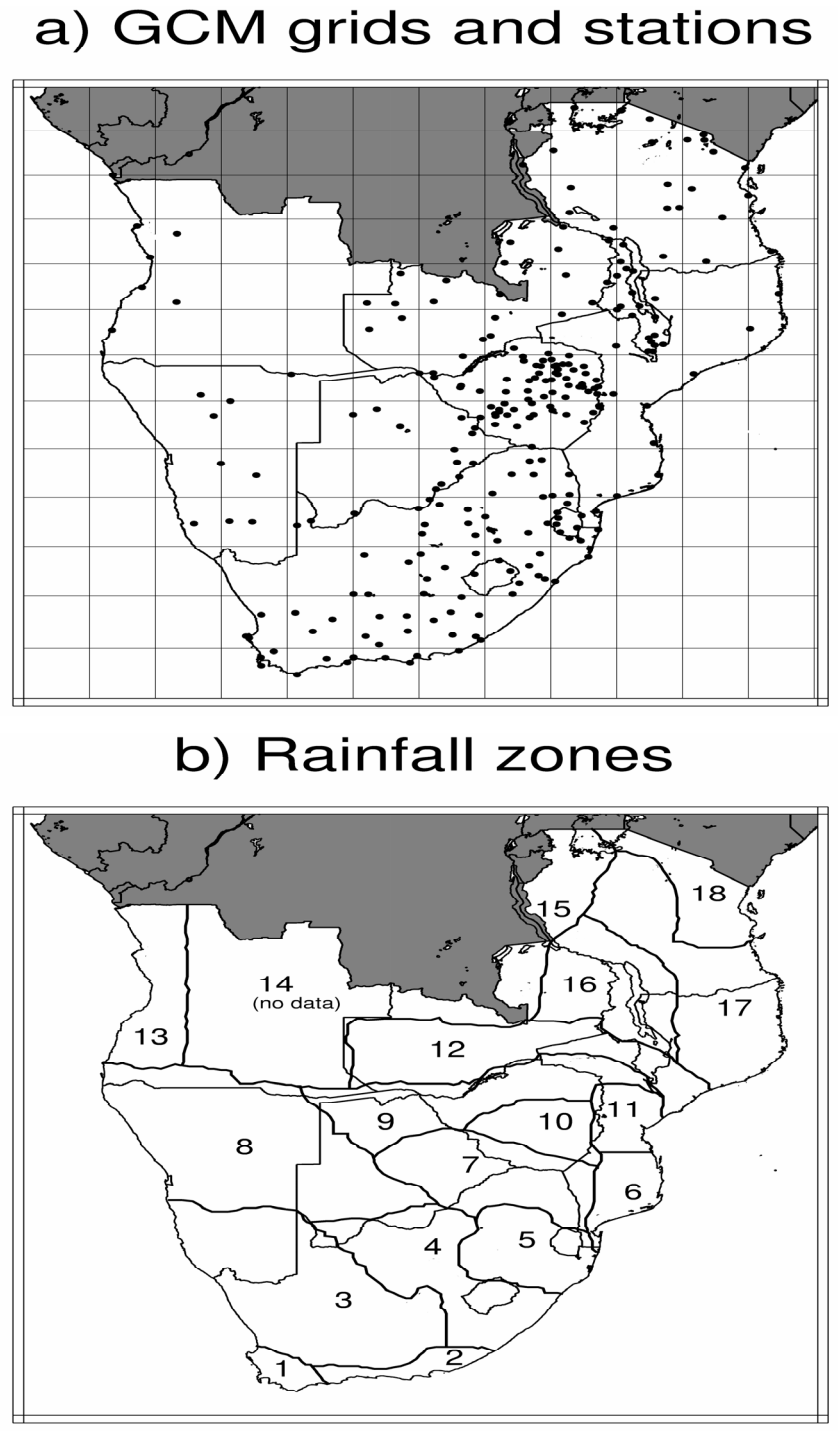


Figure 1. Location maps of the (a) 255 rainfall stations and GCM grid boxes and (b) 18 regions obtained from cluster analysis. Countries where data are unavailable are shaded. Rainfall data obtained from the SADC Drought Monitoring Centre, Harare (DMC-H).

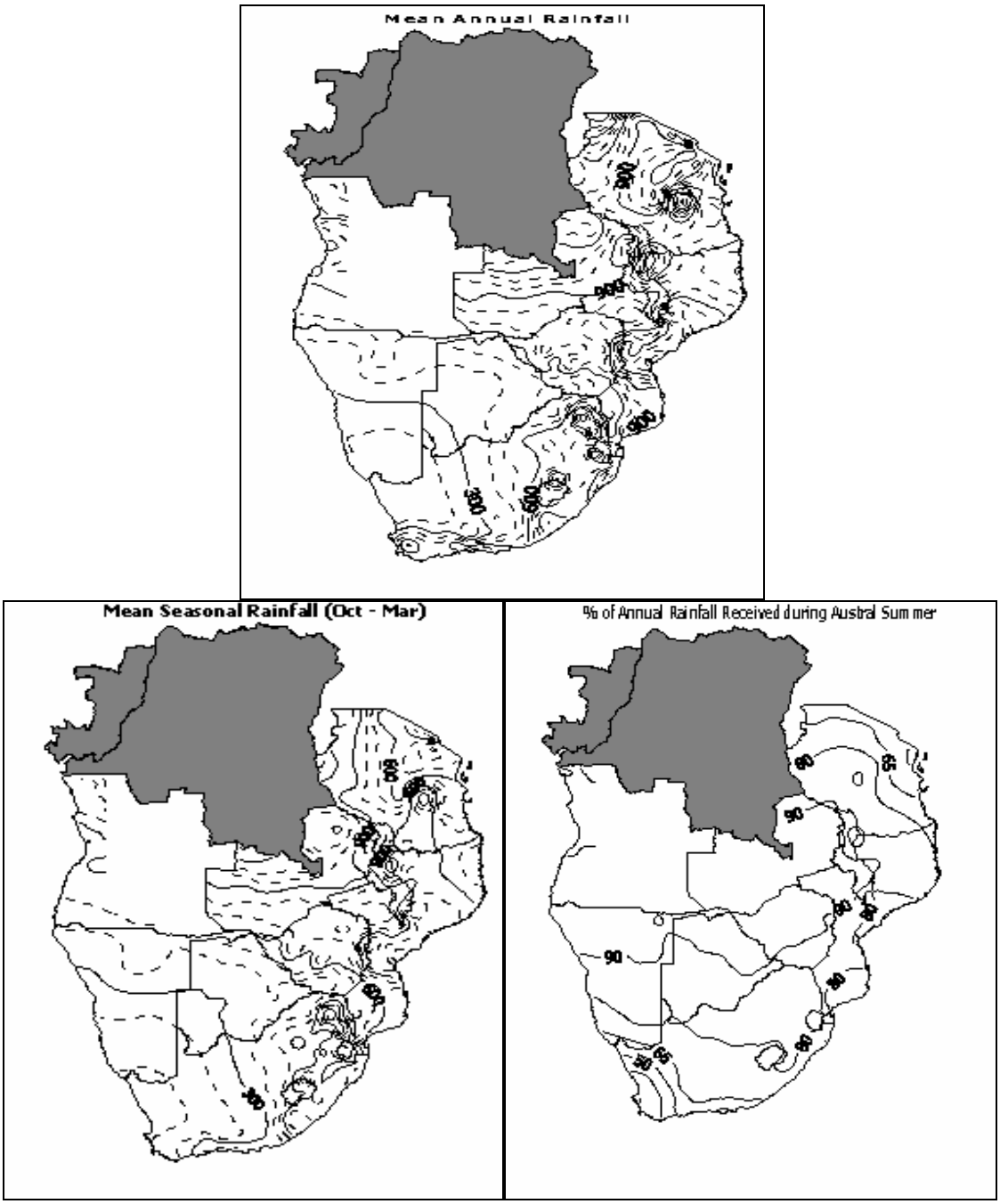


Figure 2: Long–term (1961–2000); *upper:* mean annual precipitation (mm) over the SADC region; *lower left:* mean seasonal rainfall (mm) during austral summer (October–March), and; *lower right:* percentage of total regional annual rainfall received during austral summer. For both mean precipitation maps, the contour interval is 100 mm.

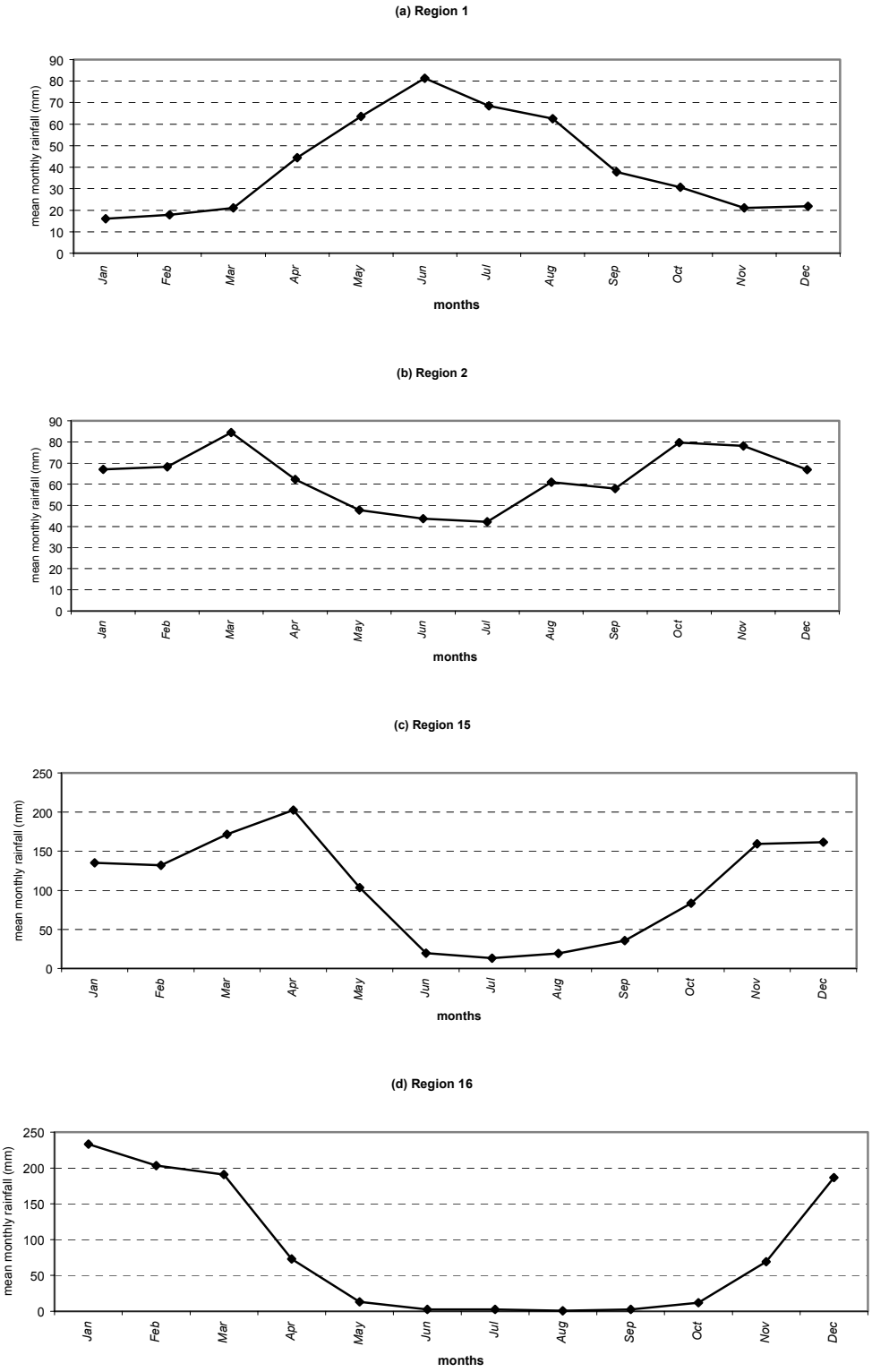


Figure 3: Examples of mean annual rainfall cycle for some selected regions over the SADC region. The locations of the regions are shown in Figure 1.

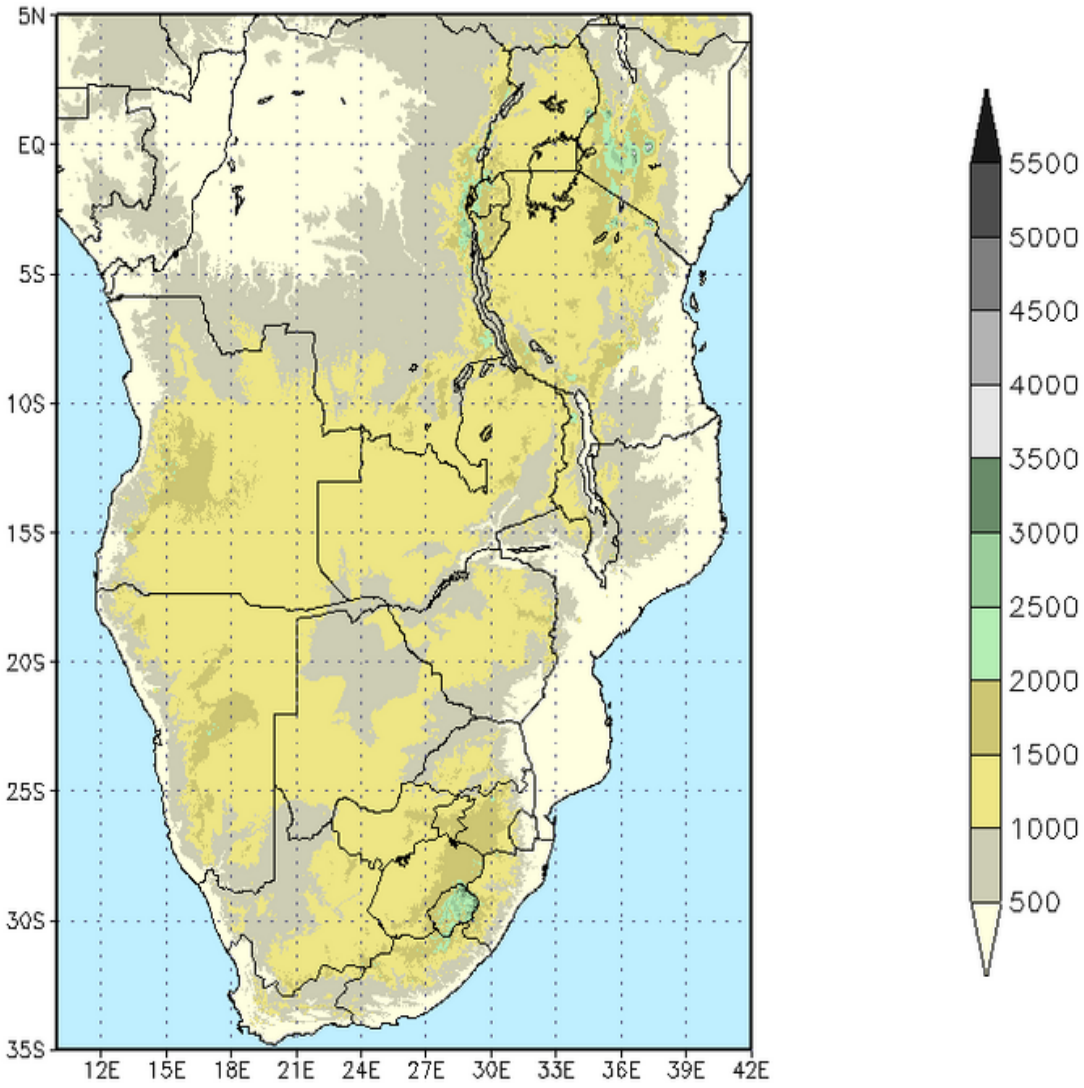


Figure 4: Topographical map of SADC. Contours are plotted at an interval of 500 m.

### *1.3.1 Sea-surface temperatures and the El Niño/Southern Oscillation (ENSO)*

A vast number of studies have associated rainfall variations over much of the SADC to large-scale features of the general circulation such as sea-surface temperature evolution (Mason 1995; Rocha and Simmonds 1997a; Tyson and Preston-Whyte 2000). The association between these slowly changing boundary conditions and austral summer rainfall has found useful application in operational long-range forecasting in the region through the use of SSTs observed prior to the season as predictors in statistical models (Barnston et al. 1996; Mason 1998; Landman and Mason 1999b).

Southern Africa interannual rainfall variability has been associated with Pacific SST anomalies such that warmer (cooler) sea-surface temperatures anomalies tend to precede suppressed (enhanced) rainfall over the southeastern sector, with the northernmost sector experiencing concurrent rainfall anomalies of the opposite sign. The spatial pattern of the Pacific SST anomalies and their temporal evolution are related to the El Niño/Southern Oscillation (ENSO) phenomenon. The influence of ENSO over the SADC region is selective, being significant over the southeastern parts of the subregion where dry (wet) conditions tend to prevail during low- (high-) phase ENSO years (Nicholson and Entekhabi 1986; Ropelewski and Halpert 1987; Nicholson and Kim 1997). Nicholson and Kim (1997) discuss seasonality in the response of regional rainfall to ENSO signals. Their results indicate that over much of the southeastern sector negative rainfall anomalies tend to occur later in the rainy season. Over equatorial East Africa, ENSO significantly modulate the 'short rains' season (OND) but exert a weaker influence on the 'long rains' (MAM). However, over the north (Zambia and Malawi), ENSO influence on rainfall weakens considerably (Rocha and Simmonds 1997a). ENSO-rainfall relationship is significant over the northernmost part (Tanzania) where positive (negative) rainfall anomalies have often occurred during El Niño (La Niña) years (Indeje 2000). Tyson and Preston-Whyte (2000) give a comprehensive description of the mechanisms and processes involved in the Pacific Ocean ENSO forcing on southern African rainfall, which accounts for about 30 per cent of the total interannual rainfall variability.

Several researchers have linked climate variability over the region to SST over the oceanic areas bordering the subcontinent (Nicholson and Entekhabi 1987; Mason 1995; Nicholson 1997; Makarau and Jury 1997; Rocha and Simmonds 1997a; Reason 1998, 2001, 2002). Nicholson and Entekhabi (1987) showed a SST spectrum for the southwestern coast of Africa (the Benguela system) dominated by strong peaks at 5 to 6 years, corresponding to the peak frequency of the Southern Oscillation, and associated with interannual rainfall variability over much of equatorial and southern Africa. Mason (1995) established a link between SST variability in the Agulhas system and the Mozambique Channel (his second principal component) (PC2) and much of the summer rainfall region of South Africa. By extrapolation, it is highly possible that this association extends to the neighbouring regions such that Agulhas warm events enhance wet conditions over much of southeastern SADC. Other ocean areas found closely linked to rainfall fluctuations include the western equatorial, and eastern and western South Atlantic (his PC3, PC5 and PC6 respectively). Findings by Rocha and Simmonds (1997a) revealed that large coherent areas of anomalously warm SSTs are often found over the tropical Pacific and Indian Oceans before and during dry summers. In agreement with Mason (1995), these authors showed evidence of a link between southeastern Africa summer rainfall and SST anomalies over the equatorial Indian Ocean independent of ENSO. Makarau and Jury (1997) identified a large area in the central Indian Ocean that is negatively correlated to Zimbabwe austral summer rainfall, with the tropical southwest Indian Ocean, east of Madagascar exhibiting correlations of the opposite sign.

A considerable amount of work has been devoted to investigating the potential influence of the subtropical south/southwest Indian Ocean SST patterns on the southern African regional atmosphere (Jury et al. 1992, 1993; Reason 1999, 2001, 2002). Jury et al. (1992) outline a Walker-type circulation linking reduced convection over the tropical southwest Indian Ocean to enhanced convection over southern Africa. The existence of interannual anomalous SST events in the South Indian Ocean not linked to the extreme phases of ENSO has been discussed by Reason (1999). These events, which normally span austral autumn of one calendar year to spring of the following year, exert a significant influence on the precipitation pattern over parts of SADC. Using the University of Melbourne

GCM, Reason (2002) demonstrated that circulation and rainfall patterns over southern Africa are sensitive to the subtropical south Indian Ocean SST dipole pattern. The results revealed that anomalously warm (cool) SSTs over the pole centred over the southwest Indian Ocean (about 28ºS, 42ºE) and anomalously cool (warm) SSTs over the southeast, off Western Australia, are associated with wetter- (drier-) than-normal conditions over southeastern Africa, and vice versa over region stretching north from Lake Malawi. This author further suggests that the influence on rainfall is dependent on the location of the southwest Indian Ocean pole relative to southeastern Africa.

These findings and others justify our use of near-global SSTs as the sole predictor in developing and running the linear statistical model. Extended reconstructed sea-surface temperatures (Smith and Reynolds 2003; 2004) are available in near real-time hence they have been found useful in operational seasonal forecasting.

### *1.3.2 The Quasi-Biennial Oscillation (QBO)*

The QBO involves a quasi-periodic reversal of lower stratospheric zonal winds from easterly to westerly phase and vice versa, with a 2–3 year periodicity. Spectral-peaks of about 2.3 years in rainfall time series have been identified for southern and equatorial Africa (Nicholson and Entekhabi 1986), and for Zimbabwe (Makarau and Jury 1997), demonstrating a link between rainfall over these areas with the QBO of stratospheric zonal winds. Previous authors (e.g. Indeje 2000; Jury et al. 1994) have discussed the relationship between the phases of QBO in the zonal wind and rainfall over eastern and southern Africa. Indeje (2000) presented evidence indicating that the westerly phase of QBO is associated with anomalously wet conditions over eastern Africa and anomalously dry conditions during its easterly phase. Jury et al. (1994) discuss a reduction in convection the southwest Indian Ocean (close to Madagascar) when the QBO is in its westerly phase.

### *1.4 Objectives*

Over southern Africa, much more effort is going into numerical model-based seasonal forecasting with the hope that dynamical models would do better than methods used previously. It is worthwhile therefore to evaluate the appropriateness of such state-of-the-art models as means to use in seasonal rainfall prediction for SADC. This study assesses the operational predictive skill of a two-tiered seasonal forecasting approach where persisted global SSTs are used to force a GCM over its integration period.

The first step in this research is to present the raw-GCM ensembles probabilistic rainfall forecast skill at smaller (regional) spatial scales. As shown in previous studies (e.g. McGuffie and Henderson-Sellers 2001), numerical climate models, while sophisticated, are still very much simpler than the climate system itself. It is expected that some form of post-processing of dynamical model output could provide optimal forecast skill. Based on this conjecture, in the next step of this study, an attempt is made to correct for model deficiencies by recalibrating the GCM simulations at regional level. The remapping of GCM output to regional rainfall is based on empirical relationships between simulated large-scale fields and rainfall. Thus regression equations are fitted and used to predict regional rainfall from larger-scale GCM simulated fields. The statistical approach employed here in fitting the recalibration equations is model output statistics (MOS) using a simpler principal components regression (PCR) and relatively complicated canonical correlation analysis (CCA) techniques. An assessment is made to determine the extent to which the recalibration methods improve the GCM forecast skill and also how they perform relative to each other. A linear statistical model linking regional rainfall to near-global SSTs is also developed. Statistical models have been used to issue seasonal forecasts of summer rainfall in Southern Africa since early 1990s, and the limits of statistical predictability have been probed. The statistical model in the context of this research therefore represents somewhat "traditional" methods and forms a baseline against which to judge the performance of more modern and sophisticated seasonal forecasting tools.

Summer rainfall over a bulk of the SADC region is somewhat erratic with significant impacts for national economies. Reliable forecasts of rainfall a month or more in advance

have obvious manifold potential benefits and would particularly be of great assistance to environmental and financial resources management. The overall objective of this research is to contribute to the efforts directed towards providing better summer rainfall forecasts for southern Africa through a combination of dynamical and statistical approaches.

Previous modelling and prediction studies for southern African summer precipitation identified certain regions where the variable has some predictability, which is however restricted to specific times of the year. To further test the validity of these inferences, the spatial variation of predictive skills has been examined over regions assumed to experience homogeneous rainfall characteristics at seasonal to interannual time scales. The main rainfall season over southern Africa (October–March) has been grouped into four three-month overlapping seasons: October–December (OND), November–January (NDJ), December–February (DJF) and January–March (JFM). The performance of the forecasting techniques is evaluated during each season so as to further examine the seasonality of the predictive skills. The effect of the lead-time on model skill is also assessed.

This report is structured as follows: In chapter 2, a brief description of the data sets used and their sources is given. The methods used in the analyses are also described. In chapter 3, an objective evaluation of the forecast schemes' performance is made. The possible sources of predictive skill are presented in chapter 4. Chapter 5 summarises and concludes the results.

# 2.0 CHAPTER 2 DATA AND METHODOLOGY

In this chapter, information about the datasets used is provided. The statistical methods used to build the prediction models are briefly described, and an explanation on how the models are evaluated is given.

## *2.1 Rainfall data and homogenous regions*

Monthly rainfall data for the 1961-2001 period has been obtained for 255 stations distributed across 11 countries within the Southern African Development Community (SADC) region. The station locations are shown in Figure 1a. The distribution of the stations is markedly irregular, most stations are concentrated over the central and southern parts with very few in the west. The rainfall data was obtained from the SADC Drought Monitoring Centre, where it undergoes quality control. Only stations with less than 5 % randomly distributed missing values are selected. Missing values are replaced using a regression method from the highest correlated neighbouring station (Tabachnick and Fidell 2001).

Homogeneous rainfall regions are defined by grouping the rainfall stations on the basis of spatial rainfall patterns that occur during the main rainfall season (October–March) over southern Africa using cluster analysis (Mason 1998; Mimmack et al. 2001). For each station, seasonal rainfall totals were calculated from October of one year to March of the following calendar year. These station seasonal totals were then used in the cluster analysis. The aim of clustering stations is to define regions within which the processes responsible for seasonal to interannual rainfall variability are similar. The clustering is based on Euclidean distances calculated from the unstandardized principal component scores (Mimmack et al. 2001). The number of retained principal components varies between 10 and 20. The higher number of principal components is retained to ensure that small but distinct regions are identified. A total of 18 regions are defined as shown in Figure 1b. No data is available over the eastern Angola (region 14); hence this region is not considered in the analysis. Notably, the clustering does not show distinct regions along the eastern coastal regions of South Africa, inconsistent with findings by previous authors (Mason 1998; Landman et al. 2001) who considered a much smaller domain

within the subregion than is used here. The present study uses too few stations over the same areas and the clustering is based on seasonal rather than annual rainfall totals, which could possibly be the source of the differences in defining the regions

In this study seasonal rainfall totals accumulated within the austral summer months are used. Three-months overlapping totals are calculated within the main rainfall season (October–March) over southern Africa. OND totals are calculated for the period 1961 to 2000, NDJ and DJF for the period 1961/62 to 2000/01, and JFM for the period 1962 to 2001. This grouping is suitable for most climate information users, such as in agriculture, who require knowledge on the expected seasonal totals and, most importantly, shifts in temporal distribution of rains within the season. While this information may not show intraseasonal rainfall characteristics such as rainfall onset, frequency and duration of dry spells, and rainfall cessation, issuing three-monthly forecasts updates during the rainy season is a standard procedure in seasonal forecasting. An investigation of the seasonal variation of the prediction skill during summer as well as its geographical distribution is therefore justified. Over southern SADC, this stratification is further necessitated by the disparate rain-bearing systems during the early and late summer months.

### *2.2 Sea-surface temperatures*

Though incorporating more variables into the predictor set may have shown an improvement in the forecast skill of statistical models (Hastenrath et al. 1995; Makarau and Jury 1997), sea-surface temperatures (SSTs) have remained the most dominant predictors for southern African summer rainfall (Barnston et al. 1996; Mason 1998; Landman and Mason 1999b). In this study, near global (60ºN–60ºS) extended reconstructed sea-surface temperatures version 2 (Smith and Reynolds 2004) are the sole predictors used for developing and running the empirical-statistical model. The SST data on a 2º x 2º lat/lon grid are extracted for the period May 1961 to November 2000 from the International Research Institute for Climate and Society (IRI) data library.

Three-month SST averages are calculated and used to establish relationships between the average SSTs prior to the rainfall season and the standardised rainfall for each homogeneous rainfall zone. Because the ECHAM 4.5 GCM forecast fields are only

available at shorter leads, the lead-time for the SST-rainfall linear models is placed between one and two months for each target seasonal rainfall period. For example, the MJJ (JJA) average SSTs and OND standardized rainfall are used to fit the CCA equations resulting in a two- (one-) month lead-time. The training period is varied for each retroactive forecast period (discussed in 2.7). Starting with a training period of *n*-years, the fitted CCA model is used to predict years *n+1, n+2,* and *n+3*. Then use *n+3* years to fit the model, which is used to predict years *n+4, n+5,* and *n+6*. In the last step *n+9* years are used to train the model from which predictions for years *n+10, n+11,* and *n+12* are made.

### *2.3 The ECHAM4.5 GCM*

The ECHAM4.5 GCM is a modified version of the ECHAM4 GCM (Roeckner et al. 1996). The hindcast mode of the GCM consisting of 12 ensemble members is used in this study. In this mode the prevailing monthly SST anomalies (serving as boundary forcing for the GCM) are persisted on top of the monthly varying seasonal cycle of SSTs for the season (three-months) of interest. The GCM predictions from this mode are valid for up to five months from the starting month (i.e. hindcasts started in month *i* are valid for that month up to month *i+4*). One- (two-) month(s) lead-time is defined when predictions for months *i+1* to *i+3* (*i+2* to *i+4*) are considered. The model grid points at a T42 spectral resolution (about 2.8º lat/lon) are shown in Figure 1a. The model rainfall predictions are averaged over all grid points located within each homogeneous rainfall region (Figure 1b).

For each training period the mean of the ensemble predictions have been calculated to get the model climate. These predictions are grouped into three categories classified as below-normal (driest third), near-normal (middle third) and above-normal (wettest third). GCM forecast probabilities are calculated by expressing as a percentage the fraction of the ensemble that fall within the upper, middle and lower categories. For example, for a 12-member ensemble GCM, if 6 ensemble members fall in the above-normal category, 3 in the near-normal, the other 3 in the below-normal, then the probability forecasts would be expressed as 50% chance, 25% chance, and another 25% chance of rainfall occurring in the above-, near- and below-normal categories, respectively.

### *2.4 The recalibration methods*

Due to systematic errors inherent in GCM simulations at regional or local scale, adjustments are necessary to improve model predictions. Model Output Statistics (MOS) using regression-based techniques is applied to model predictions in this study to improve the skill of the forecasts. The MOS approach (Wilks 1995; Landman and Goddard 2002) statistically links archived records of GCM forecast fields (considered as predictors) and historical rainfall records for the same season. The developed relationships are then used to produce MOS-based forecasts. In this approach the lead-time is incorporated through the GCM forecasts as illustrated in the foregoing section. For example, if the DJF model forecasts are produced early in October (November) then the lead-time is two (one) months. The value of the forecasts issued at these lead times is sufficiently high both practically and economically, and thus their skills are evaluated in this research.

#### *2.4.1 Principal components regression*

This method combines principal component analysis (PCA) and regression. Principal components of the predictor variables (GCM forecast fields) are regressed against the standardised rainfall anomalies. The method extracts the most important spatial modes of variability of the large-scale atmospheric GCM-simulated fields, considered as signals, and weights their influence on the seasonal distribution. In this way, the effect of locally controlled small-scale features, considered as noise is excluded. When dealing with climate data, multiple regression becomes cumbersome due to the huge datasets involved. In addition, a large number of predictors from neighbouring locations or grid points are inherently highly correlated. The high correlations among the predictor variables often result in highly unstable regression coefficients and consequently a large forecast error. Since the principal components are uncorrelated, principal components regression (PCR) eliminates the problem of multicollinearity of the predictors (Jackson 1991). In this study a regression model was developed using a limited number of dominant principal components (as determined from scree test) of the GCM forecast fields as predictors and standardised rainfall for each region (Figure 1b) as the predictand.

### *2.4.2 Canonical Correlation Analysis*

Canonical correlation analysis (CCA) (Barnett and Preisendorfer 1987; Jackson 1991; Wilks 1995; von Storch and Zwiers 1999) is similar to PCR by constructing a statistical model based on empirical relationships among variables. CCA however identifies pairs of linear combinations among the predictor and predictand variables whose time evolution is optimally correlated. The dominant CCA pair gives the highest canonical correlation, followed by the next pair and so on, subject to the condition that successive time coefficients are orthogonal to the previous ones. It is the procedure of identifying multicomponent predictors and multicomponent predictands exhibiting the strongest link that increase the complexity of CCA relative to PCR, which linearly combines only the predictor variables. In this study, CCA is used to develop the SST-rainfall statistical model as well as for recalibrating GCM forecasts. The statistical methods used in this research to construct the prediction models have been chosen because of their ability to give guidance with respect to the physical processes underlying the skilful forecasts. This is achieved through an examination of the leading modes of the predictor and predictand canonical loading patterns. The predictor loading patterns are used for a similar purpose in the case of PCR.

## *2.5 Optimal statistical model selection*

The performance of the techniques used in this study for constructing the statistical models is highly dependent on the number of principal components (PCs) retained for the PCR or CCA. In the case of CCA, the linear model is also sensitive to the number of modes used in the regression. In this research, the maximum number of predictor and predictand principal components to be retained for further analysis is determined from the scree test (Jackson 1991). The optimum number of predictors is further selected on the basis of cross-validation (Elsner and Schmertmann 1994) over the training period. Essentially cross-validation involves successively leaving out a segment of the observed data, reconstructing the prediction model, and then making predictions for the omitted cases. In this research, the cross-validation window is chosen to be five years. Using the five–year cross validation window, except for the first and last two years, all the cross-validated forecast target years are bracketed with two years both before and after. This

ensures that significant temporal autocorrelation in the predictand data, which seldom exists with data for successive seasons, and trends, do not inflate the overall cross-validated skill. Five years are left out in the training data and the model reconstructed using the *N-5* years. The model is then used to predict the middle year. The procedure is repeated successively until all the years have been predicted. The ultimate result is a set of *N* predictions, which are then compared directly with the *N* observations to estimate the model's overall skill using the correlation coefficient.

For the PCR models, the cross-validated skill was calculated, starting with only the leading principal component in the model, including the next at each step. A similar selection criterion was used for the CCA models. With the CCA modes restrained to be the minimum of the predictor and predictand retained empirical orthogonal function (EOF) modes, all the possible combinations are tested and the combination yielding the best cross-validated skill over each training period is selected.

### *2.6 Retroactive forecasting*

In order to get realistic indications of how skilful the models would be in an operational environment, the model performance is assessed over an independent testing period. In this retroactive procedure the available data are divided into two sets, the 28 years of SST data 1961-88 (and corresponding standardised rainfall anomalies for each target season) are initially chosen to be the model fitting or training period for the SST-rainfall model, and the 3 years 1989-91 for independent forecasting. After the first 3-year predictions are made, the training period is updated and the model fitted using the 31 years of SST data 1961-91, and predictions for the next 3 years made. This procedure is repeated using the optimal model (possibly consisting of different number of EOF and CCA mode combinations) until 12 retroactive predictions are made. To ensure that the observed rainfall categories corresponding to each retroactive forecast period remained equiprobable, the categories are defined from the maximum multiple-of-3 number of years in the training period. For an integer *n,* each SST-rainfall training period consisted of $3n+1$ years, which required an omission of the last year when defining the categories. For example, the OND 1961–87 (*27)* period is used as the reference climatology to define

the categories to which the observed rainfall for OND 1989–91 falls, omitting the year 1988.

For the MOS models, the initial training period is set to 21 years (1968-88). After making the first retroactive forecast for the three-year period, 1989–91, the model-fitting period is updated at regular steps of three years each until the 12 predictions are made. For each retroactive step, the model climatology is redefined from its predictions over training period. These climatologies form the basis for calculating probabilistic model forecasts from the fraction of the ensemble falling within a given tercile as discussed in section 2.3.

### *2.7 Model validation*

Due to the uncertainty inherent in long-lead forecasts, the common practice in climatology is to present the forecasts probabilistically (Goddard et al. 2001). Accordingly, in this study, the retroactive forecasts are expressed in probabilistic terms. The raw-GCM probabilistic forecasts are derived from the distribution of the ensemble members among the three categories as discussed in 2.3. For the statistical models, deterministic forecasts are converted into probabilities using contingency tables. The probabilistic forecasts are then paired with the subsequent observations for each season during the testing period, and probabilistic performance scores calculated, which are used to quantitatively validate the prediction models. The skill scores used to assess model performance are the ranked probability skill score (RPSS)(Wilks 1995; Mason and Mimmack 2002; Toth et al. 2003), and the relative operating characteristics (ROC) areas (Mason and Graham 1999; Mason 2003). These skill scores measure different aspects of forecast performance, but do not give a complete picture (Wilks, 1995). The RPSS gives an overall (all categories) measure of the skill of probabilistic forecasts, while the ROC areas indicate the ability of the forecast system to discriminate between individual categories.

#### *2.7.1 The ranked probability skill score*

The ranked probability score (RPS) is a multiple-category extension of Brier score (Wilks 1995; Toth et al. 2003). The RPS measures squared differences between forecast and

observed cumulative probabilities. This metric gives the overall performance over all three categories such that forecasts issuing higher probabilities to categories leaning towards observations are awarded high credit and are severely punished if the high probabilities are assigned to those categories further away from the observed. For K number of categories, the RPS for a single forecast/event pair is given by

$$RPS = \sum_{n=1}^{K} \left[ \left( \sum_{i=1}^{n} f_i \right) - \left( \sum_{i=1}^{n} o_i \right) \right]^2 \qquad (1)$$

(Wilks 1995). Here, for each realisation $i$, $f_i$ is the forecast probability of the occurrence of the event, and $o_i$ is the outcome, which equals 1 or 0 depending on whether or not the event occurred (Wilks 1995; Toth et al. 2003). In this study, the number of forecast categories $K = 3$ and the overall RPS for a forecast system is obtained by averaging that obtained in Eq. 1 over the n = 12 years. The RPS is negatively oriented, with the best score of zero obtained for a perfect forecast system, and positive scores further away from zero are indicative of a systematically erroneous forecast system.

The RPS can be converted to a skill score the ranked probability skill score (RPSS), which compares the ranked probability score of the forecast system ($RPS_{fcst}$), to that of a reference forecast strategy ($RPS_{ref}$) as

$$RPSS = 1 - \frac{RPS_{fcst}}{RPS_{ref}} \qquad (2)$$

(Wilks 1995). This score measures the level to which the forecast strategy in use outperforms that of a simpler and presumably low skill forecast strategy (Goddard et al. 2003). The possible range of RPSS is [-∞, 1], such that it is positive (negative) for a forecast system that performs better (poorer) than the reference system (Toth et al. 2003). The most commonly used reference strategies are climatology, in which the prior probability of the event being forecast is issued perpetually and to a lesser extent random

guessing, where the outcome is independent of the forecast (Mason 2004). Intuitively, using a climatological forecasts as reference strategy is appealing given that it gives an indication of how necessary the forecasts are compared to just knowledge of the historical probabilities of the event. Using the Brier skill score (BSS), Mason (2004) showed that using climatology as reference strategy can result in negative skill scores when the variance of the forecast probabilities about those of climatology is high. Thus this reference may hide some potentially useful information in the forecasts. Random guessing in which the forecasts are randomly shuffled such that the observed outcome is independent of the forecast probabilities is an alternative reference strategy which adjusts the forecast's sharpness. However this strategy is not strictly proper. For details of the advantages and disadvantages associated with each reference strategy the reader is referred to Mason (2004). In this research skill scores for the competing forecast systems are calculated with reference to both strategies.

### *2.7.2 The relative operating characteristics score*

The ROC curve gives a useful indication of the forecast system's ability to discriminate between alternative outcomes. The curve is based on a comparison of conditional relative frequencies of issued warnings (W) given that the event (E) occurred (i.e. p(W|E), also called hit rate) and those of warnings issued prior to non-occurrence (E') of events (i.e. p(W|E'), also called the false-alarm rate). These ratios are plotted on a unit square, the hit rate (HR) on the ordinate and the false-alarm rate (FAR) on the abscissa. The locus of points on the unit square (the ROC curve) depends on the forecast systems ability to correctly anticipate the occurrence or non-occurrence of predefined events.

The most commonly used ROC-based score is the area under the curve also referred to as the ROC score (Mason and Graham 1999). ROC score's possible range is [0,1], with a score of 1 indicating perfect skill. For a forecast system that accumulates more hits at the expense of false alarms, the curve will lie above the southwest to northeast diagonal (the 0.5 line) indicating potentially useful forecasts. A ROC curve falling along the 0.5 line (HR = FAR) is obtained for a forecast system with no skill (Mason and Mimmack 2002). Scores less than 0.5 are indicative of forecasts with negative skill.

The ROC score gives estimates of forecast skill for individual categories. Hence these scores are calculated for each of the three categories separately. However, it is only forecasts of the two extreme categories that are of concern to society. Accordingly, only results for the above- and below-normal categories will be presented in this report. In any case, the skill scores for predicting the near-normal category are very low.

### *2.8 Significance tests*

To test for the statistical significance CCA spatial patterns, the differences in the cross validated fit using different potential predictor variables from the GCM output fields, a Monte Carlo or resampling technique (Wilks 1995) has been applied. In this non-parametric approach to significance testing, 1000 artificial batches of the same size at the actual data are constructed using time-shuffled versions of the original rainfall data. A CCA is performed between the predictor data and each batch of resampled predictand data to obtain a null distribution of the test statistic. For each grid, the loadings are sorted in ascending order. From the 1000 ranked values, the $950^{th}$ is used as the 95% confidence level critical value. A similar procedure has been followed to test the significance in the difference between the cross-validated correlations obtained using the potential predictor variables in the MOS models.

# 3.0 CHAPTER 3 PREDICTABILTY OF SEASONAL RAINFALL OVER SOUTHERN AFRICA USING RAW-GCM ENSEMBLES, A LINEAR MODEL AND MODEL OUTPUT STATISTICS

This study compares the performances of two regression-based recalibration methods relative to each other as well as to some competitive baseline forecasting schemes. In this chapter we show the ranked probability skill scores (RPSS) and the relative operating characteristic (ROC) scores for each of the competing forecast tools per given target season.

## *3.1 Previous related research*

Over the past two decades there has been a notable improvement in our ability to forecast seasonal rainfall anomalies over southern Africa. Dynamical and statistical models have been applied with success, so are recalibration techniques. The methods used in this research have been successfully applied over parts of southern Africa and elsewhere. In this section some useful results are reviewed.

### *3.1.1 Purely-statistical models*

Previous researchers have investigated the predictability of rainfall over southern Africa using statistical methods (e.g. Hastenrath et al. 1995; Barnston et al. 1996; Makarau and Jury 1997; Mason 1998; Landman and Mason 1999b; Unganai and Mason 2002). Except for Barnston et al. (1996), these studies considered a limited southern African sector.

The performance of three statistical methods was assessed by Hastenrath et al. (1995) in predicting rainfall over northeastern South Africa during the peak austral summer season. Although confined to a very narrow domain, their study demonstrates that incorporating more predictor variables into a statistical model such as indices of lower- and upper-atmospheric circulation improves the model skill. Amongst the statistical methods used in their study, neural networks were clearly superior indicating that important relationships among climate variables, which find useful applications in operational seasonal to interannual climate prediction, are not essentially linear. Makarau and Jury (1997) further demonstrate the importance of using multiple predictor variables in statistical modelling.

Their study considered sea-surface temperatures, the Southern Oscillation index (SOI), the Quasi-biennial Oscillation (QBO), outgoing long-wave radiation (OLR) and wind observed in spring as possible indicators of the next-seasons' shift in summer rainfall anomalies over Zimbabwe. They found usable skill in predicting early and late summer rainfall. Mason (1998) presented a non-linear discriminant analysis model, which indicated high predictability of the tropical atmosphere. Highest forecast skill was obtained over much of the austral summer rainfall region of South Africa.

Using evolving patterns in four prior consecutive 3-month SST fields as predictors into a CCA model, Barnston et al. (1996) found usable skill in predicting January–March (JFM) rainfall over isolated areas in southern Mozambique, central Malawi and parts of Zimbabwe. Their study only used individual station observations and the data were quite sparse over much the SADC region. In this research, regionally averaged rainfall is used instead, to minimize the influence of spatial noise and the effect of sparse observing stations over some parts of the region, particularly to the west. Using a similar approach to that of Barnston et al. (1996), Landman and Mason (1999b) found higher skill in forecasting the late austral summer (January–March) rainfall over South Africa than earlier in the season (October–December). One possible reason to this is the dominance of forced atmospheric variability during the peak of the rainy season, in contrast to the early part of the season when atmospheric internal variability, which is chaotic, dominates. Here a more broad and comprehensive evaluation of the spatial and temporal dependence of forecast skill is made over almost the whole of SADC using operationally viable methods that most National Meteorological Services are now capable of handling.

### *3.1.2 Numerical Models*

General circulation models have been applied with some success in the production of operational monthly to seasonal climate forecasts over many parts of the globe including southern Africa (Joubert 1997; Rocha and Simmonds 1997b; Tennant 1999; Barnston et al. 2003; van Oldenborgh et al. 2004). These climate prediction tools are quite complex and not very popular in many SADC National Meteorological Services mainly due to computational constraints.

An assessment of the ability of seven low-resolution Atmospheric Model Intercomparison Project (AMIP) GCMs to simulate Southern Hemisphere circulation features that exert an important influence on southern African climate, and their representation of summer rainfall from 1979 to 1988 has been carried out (Joubert 1997). The results revealed that the models simulate circulation features quite well, better than earlier GCMs (Joubert 1995), but were not equally skilful in simulating rainfall patterns such as mean annual rainfall cycle and JFM interannual rainfall variability during the testing period. Using a four-member ensemble Melbourne University General Circulation Model in which SST anomalies were prescribed as lower boundary forcing, Rocha and Simmonds (1997b) found that positive SST anomalies in the tropical Indian Ocean are the most important oceanic forcing causing dry summers over eastern SADC. Anomalously warm SSTs over the central Indian Ocean are favourable for low-level cyclonic circulation east of Madagascar, which deprives the eastern parts of meaningful moisture as trade winds, and monsoonal airmasses tend to be diverted towards the ocean. Their results also showed that the atmosphere responded slightly stronger when either Pacific and/or the south Indian Oceans SSTs were prescribed. The performance of the Centre for Ocean-Land-Atmosphere Studies (COLA) T30L18 GCM in forecasting monthly climate for southern Africa has been examined (Tennant 1999). The results demonstrated that the low-resolution GCM produce skilful monthly forecasts higher than for persistence. Correcting for grid point biases for each month based on known model drift enhanced the forecast skill.

It has been noted that no single climate model is capable of simulating all atmospheric fields adequately. Attempts are therefore being made to combine output from different atmospheric general circulation models (AGCMs) into a single forecast (e.g. Barnston et al. 2003; Robertson et al. 2004). Earlier approaches involved weighting the model predictions unequally according to their historical performance. Recently, objective multimodel ensembling techniques such as the Bayesian and canonical variate methods have been devised (Barnston et al. 2003). Consolidating predictions from several GCMs, while effective, does not offer a huge improvement in forecast skill, but performs equally well or just slightly better than the most skilful AGCM in the set. There have been

suggestions that additional empirical tools could still play an important complementary role when used in parallel with the best combination of AGCMs (Barnston et al. 2003).

### *3.1.3 Recalibration methods*

Progress made with combining dynamical and statistical approaches has enabled a regular production of climate forecasts that are based on statistical recalibration of GCM output (Karl et al. 1990; von Storch et al. 1993; Zorita and von Storch 1999; Landman and Tennant 2000; Busuioc et al. 1999, 2001; Landman et al. 2001; Landman and Goddard 2002; Mo and Stratus 2002). For some parts of the SADC region and in many cases, recalibration methods improve upon the skill realised from dynamical climate models' rainfall forecasts (Landman and Goddard 2002).

Using CCA to recalibrate large-scale circulation forecasts by the COLA T30 GCM to regional rainfall for 30-day periods over South Africa, Landman and Tennant (2000) found high skill over much of the interior and eastern coast. Furthermore, extreme events were captured adequately by the MOS technique. Using a perfect prognosis approach to recalibrate bias-corrected simulations of circulation and moisture for the same GCM (COLA) to produce seasonal rainfall forecasts for some regions in southern Africa, Landman et al. (2001) found high skill for the GCM-based approach at shorter lead-times, outscoring the baseline skill formed using a linear statistical method. However, at longer lead times, the GCM-based system performed least well. Landman and Goddard (2002) used the MOS technique to recalibrate the ECHAM 3.6 GCM (an earlier version of the GCM used in this study) 850-hPa geopotential height fields to regional rainfall over southern Africa. Their study used both the simulation and hindcast modes of the GCM. In the simulation mode the GCM was forced using simultaneous observed SSTs while in the hindcast mode the GCM was forced with monthly SSTs for the previous month persisted on top of the monthly varying seasonal SST cycle. The MOS-recalibrated forecasts outperformed the area-averaged GCM-simulated rainfall forecasts as well as predictions obtained from a linear statistical model. Significant MOS skill was found over much of the austral summer rainfall regions.

In this research, an approach similar to Landman and Goddard (2002) is adopted for a much larger domain. A related but simpler PCR-MOS technique is also applied and compare with the methods used in the reference paper. The following sections present the results obtained from the various methods of analysis.

### *3.2 Optimal model selection*

The GCM hindcast fields considered as candidate predictors for the MOS models were the geopotential heights (1000-, 850-, 700-, and 500-hPa), total precipitation, and total cloud cover. The difference in cross validated correlation over the four model fitting periods using each GCM output field as a predictor in the MOS models is noticeable, albeit small. Amongst all the potential predictors, the 850-hPa geopotential height proved the best predictor of austral summer rainfall over southern Africa, consistent with findings by Landman and Goddard (2002). The 700-hPa geopotential height field is the second best predictor, followed by 1000-hPa, and then 500-hPa. The GCM total precipitation and cloud cover produced the least overall skill. However, the rerandomization tests rendered the differences between the cross validated skill scores obtained using each forecast field as predictor in the MOS models statistically insignificant at the 95% confidence level. For example, for DJF rainfall forecasts issued at one- (two-) month lead-time, the 21-year training period associated with a 95% confidence level threshold of cross-validated correlation difference between the 850-hPa geopotential height and total cloud cover of 0.1031 (0.1816), the 24-year period with 0.1391 (0.2031), the 27-year period with 0.1087 (0.2308), and the 30-year period with 0.1319 (0.2517). The actual differences in cross-validated correlation do not exceed these critical values.

The 850-hPa geopotential height field is acceptably well simulated by the GCM and hence appropriate as a predictor of regional rainfall. Much of SADC is more than 1000 m above mean-sea-level, thus the 850-hPa should provide a good representation of low-level synoptic circulation, which is one of the dominant factors determining regional climate variability over the interior plateau.

The selected optimal combination of predictor and predictand EOF modes retained in the CCA analysis, and the number of CCA pairs used in each statistical model are presented in Table 1. The training periods (defined according to the length of the predictor data), target periods and their corresponding lead times are also shown. The goodness index is expressed in the terms of the correlation coefficient.

For the linear statistical model, there is consistency in selecting the number of SST and rainfall EOFs, and the CCA modes making up the optimal model for each training period. There are only minor differences in the combination making up the optimal model for the 1961-97 training period. This consistency makes sense given that the training periods have many years in common. For the CCA-MOS models however, the number of the EOFs and CCA modes change each time the training period is updated.

The correlation coefficients for the CCA-MOS models are relatively higher than for the linear statistical model at all lead times. Though this could suggest higher (but not essentially statistically significant) spatial correlation between GCM 850-hPa geopotential height fields over some grids and regional rainfall, it is possible that these correlations are greater only by chance since the data length is not uniform.

The optimum number of principal components (PCs) of the predictor field used in the PCR model is shown in Table 2. The number of skilful predictor PCs ranges from 2 to 5. In each case, about 58 % of the total variance is explained by the first two leading modes. In this study the PCs are entered into the model according to the magnitudes of their associated characteristic roots. Though the first mode in each case appeared the most important predictor, the selection criteria used is designed to ensure that additional PCs would only be allowed into the model if they make a positive contribution to the forecast skill.

### *3.3 Performance of the models*

In this section the skill scores for predicting each of the three-month overlapping seasons are presented. Before presenting the potential predictability for each of the three-month overlapping seasons using the methods tested in this study, it is worthwhile to note that each season is of some agricultural, economical and societal importance. October–December marks the onset of the rainy season over much of SADC, with highest rainfall amounts received over the southern parts (from extratropical systems) and the northern parts (due to ascent associated with the ITCZ). The rainfall distribution within this season is crucial for planting of most cash crops, which typically occurs early in November. November–January rainfall is critical in sustaining crops during their vegetative stage. Flowering, tasselling and grain filling typically occur around January/February. The rainfall distribution during the peak (December–February) and late (January–March) is therefore crucial during these most-sensitive stages of crops.

#### *3.3.1 October–November–December season*

The average RPSS for each region over the 12-year retroactive period OND 1989–2000 calculated at one- and two-months lead times are shown in Figure 5. The baseline skill of the raw-GCM ensemble forecasts and CCA linear statistical model are also plotted to allow a visual comparison of the scores. The top two graphs (a,b) show the RPSS at two- and one-month lead times calculated relative to a strategy of perpetually issuing climatological probabilities for each of the three categories, whereas the bottom two (c,d) are based on a strategy of random guessing.

Using a reference strategy based on climatology, positive skill is found with all the forecast tools save the raw-GCM over much of the southern parts of SADC (Regs. 3, 4, 5, 6, 7, 8) at two-month lead-time. At a one-month lead-time, the skill is higher over the same regions and even over the northernmost region. This is indicative of predictive skill exceeding that of climatological forecasts. Notably, all the predictive tools except for very few cases surpass the RPSS for the raw-GCM ensembles. The predictability of OND rainfall over much of central and northern parts is low as indicated by negative scores where model forecasts have difficulties outscoring the reference climatology forecasts.

The central parts are typically drier during October before the ITCZ reaches its southernmost surface position in December/January. Most regions documented as potentially predictable during OND (e.g. Landman and Mason 1999b) appear to have positive skill even in this study. The models however attain positive scores when compared with a strategy of random guessing (Fig. 5c,d), particularly at a shorter lead-time. In fact, stronger positive skill is obtained for all the models when compared against this reference, suggesting that the climatological forecasts are more difficult to beat than randomly guessing the possible outcome. For the other models except for the GCM, the skill is positive over most regions. Of all the models, the PCR-MOS model, while not clearly superior to the CCA-MOS, appears to provide the best forecasts. During OND, the linear statistical model competes well with the other tools over the summer rainfall region of South Africa (Regs. 3, 4, 5 and 7). This result is consistent with Landman and Mason (1999b), who found significant cross-validated forecast skill over the same area applying the same model but using evolving SST predictor patterns instead.

The ROC scores (area under the ROC curve) for the same season are plotted in Figure 6. The top two graphs (a,b) show the ROC scores for two-month lead forecasts for the below- and above-normal categories and the bottom two (c,d) show scores for the forecasts issued in September. The ROC score is a less stringent measure, which does not penalize over- and under-confidence. It can give a high score even if the forecast probabilities do not correspond with the observed probability of an event (Mason and Mimmack 2002). In general, the ROC scores reveal a similar but more optimistic picture than the RPSS, with additional information on predictability of above- and below-normal conditions not evident from the RPSS.

TABLE 1. The different combinations of the number of predictor and precipitation (prcp) EOFs, and the number of CCA modes used in the CCA statistical models developed for each retroactive period

| | | | **Number of EOF Modes** | | | |
|---|---|---|---|---|---|---|
| *Target Season* | *Training Period* | *Lead-time (months)* | *SST* | *PRCP* | *CCAs* | *Correlation coefficient* |
| **OND** | 1961-88 | 2 | 10 | 5 | 2 | 0.071 |
| | 1961-91 | 2 | 9 | 6 | 3 | 0.043 |
| | 1961-94 | 2 | 6 | 7 | 6 | -0.002 |
| | 1961-97 | 2 | 10 | 7 | 2 | -0.044 |
| | 1961-88 | 1 | 10 | 5 | 5 | 0.127 |
| | 1961-91 | 1 | 9 | 7 | 6 | 0.115 |
| | 1961-94 | 1 | 9 | 5 | 5 | 0.084 |
| | 1961-97 | 1 | 10 | 3 | 2 | 0.079 |
| | | | *850-hPa* | *PRCP* | *CCAs* | |
| | 1968-88 | 2 | 9 | 3 | 3 | 0.177 |
| | 1968-91 | 2 | 2 | 3 | 2 | 0.039 |
| | 1968-94 | 2 | 2 | 2 | 2 | 0.015 |
| | 1968-97 | 2 | 2 | 3 | 2 | 0.038 |
| | 1968-88 | 1 | 2 | 3 | 2 | -0.021 |
| | 1968-91 | 1 | 8 | 4 | 4 | 0.060 |
| | 1968-94 | 1 | 9 | 5 | 3 | 0.094 |
| | 1968-97 | 1 | 2 | 3 | 2 | 0.038 |
| | | | *SST* | *PRCP* | *CCAs* | |
| **NDJ** | 1961-88 | 2 | 9 | 2 | 2 | 0.068 |
| | 1961-91 | 2 | 10 | 4 | 3 | 0.006 |
| | 1961-94 | 2 | 8 | 4 | 3 | 0.097 |
| | 1961-97 | 2 | 7 | 6 | 3 | 0.066 |
| | 1961-88 | 1 | 7 | 4 | 4 | 0.051 |
| | 1961-91 | 1 | 8 | 4 | 4 | 0.114 |
| | 1961-94 | 1 | 8 | 4 | 4 | 0.126 |
| | 1961-97 | 1 | 8 | 5 | 3 | 0.094 |
| | | | *850-hPa* | *PRCP* | *CCAs* | |
| | 1968/69-88/89 | 2 | 5 | 2 | 2 | 0.214 |
| | 1968/69-91/92 | 2 | 5 | 2 | 2 | 0.246 |
| | 1968/69-94/95 | 2 | 6 | 4 | 3 | 0.264 |
| | 1968/69-97/98 | 2 | 3 | 2 | 2 | 0.241 |
| | 1968/69-88/89 | 1 | 3 | 2 | 2 | 0.242 |
| | 1968/69-91/92 | 1 | 4 | 2 | 2 | 0.267 |
| | 1968/69-94/95 | 1 | 3 | 2 | 2 | 0.230 |
| | 1968/69-97/98 | 1 | 4 | 1 | 1 | 0.161 |
| | | | *SST* | *PRCP* | *CCAs* | |
| **DJF** | 1961-88 | 2 | 8 | 5 | 5 | -0.049 |
| | 1961-91 | 2 | 8 | 5 | 5 | -0.013 |
| | 1961-94 | 2 | 8 | 6 | 5 | 0.019 |
| | 1961-97 | 2 | 5 | 4 | 3 | 0.022 |
| | 1961-88 | 1 | 7 | 5 | 5 | 0.009 |
| | 1961-91 | 1 | 8 | 5 | 5 | 0.015 |
| | 1961-94 | 1 | 6 | 5 | 5 | 0.041 |
| | 1961-97 | 1 | 6 | 3 | 3 | 0.061 |
| | | | *850-hPa* | *PRCP* | *CCAs* | |
| | 1968/69-88/89 | 2 | 5 | 3 | 2 | 0.047 |
| | 1968/69-91/92 | 2 | 5 | 6 | 3 | 0.091 |
| | 1968/69-94/95 | 2 | 3 | 4 | 1 | 0.117 |
| | 1968/69-97/98 | 2 | 3 | 1 | 1 | 0.112 |
| | 1968/69-88/89 | 1 | 5 | 3 | 2 | 0.267 |
| | 1968/69-91/92 | 1 | 5 | 5 | 2 | 0.295 |
| | 1968/69-94/95 | 1 | 4 | 1 | 1 | 0.257 |
| | 1968/69-97/98 | 1 | 4 | 1 | 1 | 0.251 |

TABLE 1 (Continued).

| *Target Season* | *Training Period* | *Lead-time (months)* | **Number of EOF Modes** *SST* | *PRCP* | *CCAs* | *Correlation coefficient* |
|---|---|---|---|---|---|---|
| **JFM** | 1961-88 | 2 | 9 | 4 | 3 | -0.139 |
| | 1961-91 | 2 | 6 | 6 | 2 | -0.149 |
| | 1961-94 | 2 | 4 | 3 | 2 | -0.089 |
| | 1961-97 | 2 | 3 | 6 | 3 | -0.002 |
| | 1961-88 | 1 | 9 | 4 | 2 | -0.040 |
| | 1961-91 | 1 | 9 | 6 | 2 | -0.041 |
| | 1961-94 | 1 | 6 | 6 | 2 | -0.030 |
| | 1961-97 | 1 | 6 | 3 | 2 | 0.043 |
| | | | *850-hPa* | *PRCP* | *CCAs* | |
| | 1969-89 | 2 | 4 | 7 | 2 | 0.063 |
| | 1969-92 | 2 | 4 | 6 | 1 | 0.056 |
| | 1969-95 | 2 | 3 | 5 | 1 | 0.115 |
| | 1969-98 | 2 | 4 | 2 | 2 | 0.173 |
| | 1969-89 | 1 | 6 | 6 | 2 | 0.042 |
| | 1969-92 | 1 | 5 | 2 | 2 | -0.040 |
| | 1969-95 | 1 | 6 | 2 | 2 | -0.023 |
| | 1969-98 | 1 | 5 | 2 | 2 | -0.018 |

TABLE 2. The optimal number of dominant GCM 850-hPa geopotential heights EOF modes used in the PCR recalibration models developed for each retroactive period

| *Target Season* | *Training Period* | *Lead-time (months)* | **Number of EOF Modes** *850-hPa* | *Correlation coefficient* |
|---|---|---|---|---|
| **OND** | 1968-88 | 2 | 4 | 0.068 |
| | 1968-91 | 2 | 6 | -0.001 |
| | 1968-94 | 2 | 2 | -0.001 |
| | 1968-97 | 2 | 2 | -0.027 |
| | 1968-88 | 1 | 5 | -0.046 |
| | 1968-91 | 1 | 7 | 0.033 |
| | 1968-94 | 1 | 6 | -0.010 |
| | 1968-97 | 1 | 6 | 0.015 |
| **NDJ** | 1968/69-88/89 | 2 | 5 | 0.148 |
| | 1968/69-91/92 | 2 | 6 | 0.188 |
| | 1968/69-94/95 | 2 | 6 | 0.115 |
| | 1968/69-97/98 | 2 | 6 | 0.116 |
| | 1968/69-88/89 | 1 | 5 | 0.224 |
| | 1968/69-91/92 | 1 | 5 | 0.247 |
| | 1968/69-94/95 | 1 | 6 | 0.216 |
| | 1968/69-97/98 | 1 | 4 | 0.112 |
| **DJF** | 1968/69-88/89 | 2 | 4 | 0.011 |
| | 1968/69-91/92 | 2 | 5 | 0.035 |
| | 1968/69-94/95 | 2 | 5 | 0.024 |
| | 1968/69-97/98 | 2 | 5 | 0.031 |
| | 1968/69-88/89 | 1 | 4 | 0.201 |
| | 1968/69-91/92 | 1 | 5 | 0.195 |
| | 1968/69-94/95 | 1 | 5 | 0.154 |
| | 1968/69-97/98 | 1 | 2 | 0.180 |
| **JFM** | 1969-89 | 2 | 4 | -0.012 |
| | 1969-92 | 2 | 4 | -0.042 |
| | 1969-95 | 2 | 3 | 0.088 |
| | 1969-98 | 2 | 4 | 0.124 |
| | 1969-89 | 1 | 6 | -0.042 |
| | 1969-92 | 1 | 5 | -0.051 |
| | 1969-95 | 1 | 5 | -0.024 |
| | 1969-98 | 1 | 4 | -0.053 |


Figure 5. Ranked probability skill scores for retroactive OND forecasts at one- and two- month lead-time. The skill scores have been based on both climatology (a,b) and random guessing (c,d) as reference strategies. The black bars represent the scores for the raw-GCM ensembles, the white dotted bars (second series) for the CCA linear statistical, the dark grey bars (third series) scores for the PCR-MOS model, and the light grey bars with several dots (fourth series) represent scores for the CCA-MOS model.

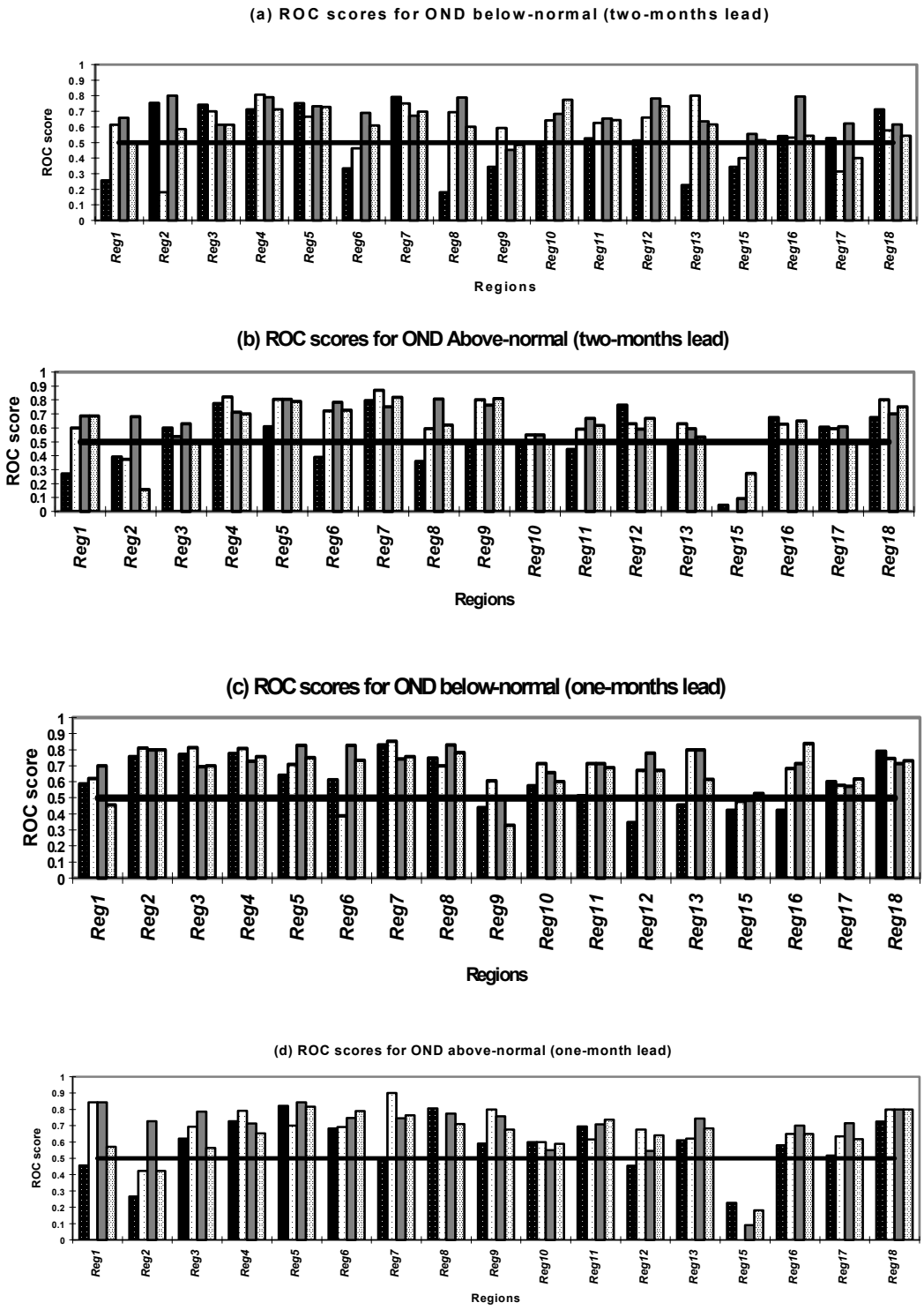


Figure 6. ROC areas for retroactive forecasts for raw-GCM ensembles (black bars), the white dotted bars (second series) for the CCA linear statistical, the dark grey bars (third series) scores for the PCR-MOS model, and the light grey bars (fourth series) represent scores for the CCA-MOS model. The 0.5 line is drawn in each case.

The scores indicate high predictability of anomalous rainfall events by all the models at both lead-times over the southeastern parts. The predictability of the extreme events weakens over the northern parts. Interestingly, even the GCM, which has been found to be the least overall performer, is able to simulate dry and wet conditions with some skill. It could be that over the southeastern areas, the atmosphere showed a typical response to anomalous SST boundary conditions (used to force the atmospheric GCM) during the below- and above-normal seasons included in the testing period. Comparing the skills for the models reveal that, with the exception of the GCM, all the models are likely to produce reliable forecasts of anomalous OND rainfall events over most regions, apart from a few regions (notably Region 15) where the predictability is poor. The skill scores for the near-normal category are not presented because the skill for forecasting this category, which is of lesser concern to end-users, is low. Despite the existence of discrepancies in model skill, no single model appears to be clearly the best forecasting tool for the entire region.

### *3.3.2 November–December–January season*

Figure 7 contains the RPSS for each model in predicting NDJ rainfall. The graphs are arranged in a manner similar to the OND case. Inspection of the graphs indicates that the models have higher skill in predicting NDJ rainfall than OND. Positive skill exists over a majority of regions including much of the previously poorly predicted central parts. Over the northern regions, except for Region 18, the predictability is low as well as over the semi-arid areas encompassing the Kalahari and much of northern Namibia at a one-month lead-time. Even during this season, the GCM ensembles are surpassed by all the forecasting tools and attain positive scores only over isolated regions. Again, the models find the reference strategy of random guessing easier to beat than climatology. Against this reference, high positive scores are observed for all the tools over all but very isolated regions. During this season there is a noticeable difference in the skill scores for the individual models, with the PCR-MOS model generally producing the most skilful forecasts.

The models ability to forecast below- and above-normal NDJ rainfall is shown in Figure 8. The relatively high predictability of anomalously dry conditions over most regions is evident from the fact that the ROC scores for the best performing models are high exceeding 0.5 in more than 70 per cent of the regions. The raw-GCM ensembles continue to be the tool with lowest overall skill in simulating anomalous rainfall during the testing period. However, there is some indication of skill in simulating below-normal NDJ rainfall, even by the GCM. This is particularly true over the southeastern parts, an area where rainfall appears to have the highest predictability, suggesting that the raw-GCM rainfall forecasts can still be useful at the regional scales considered in this study.

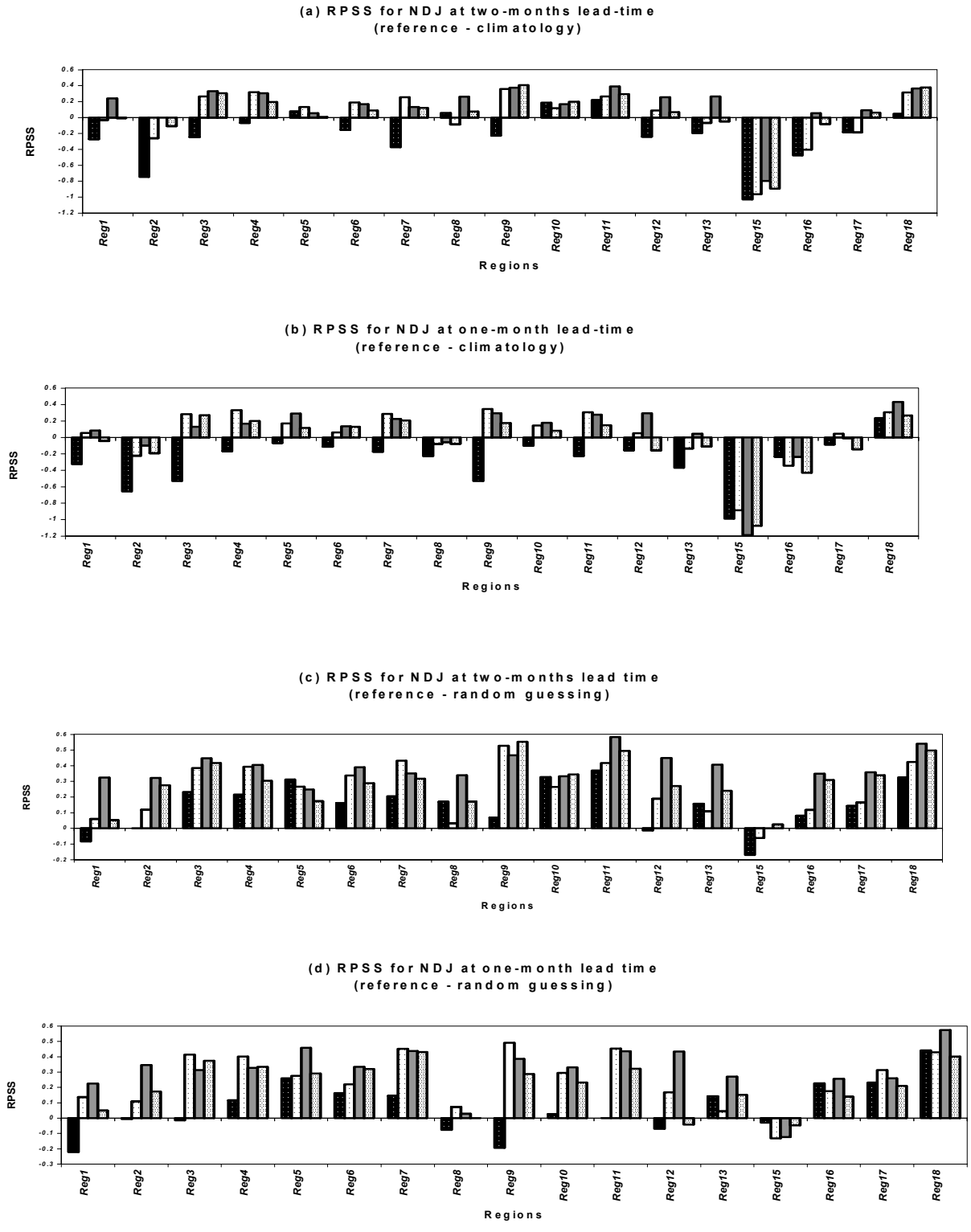


Figure 7. Same as Figure 5, but for the NDJ season.

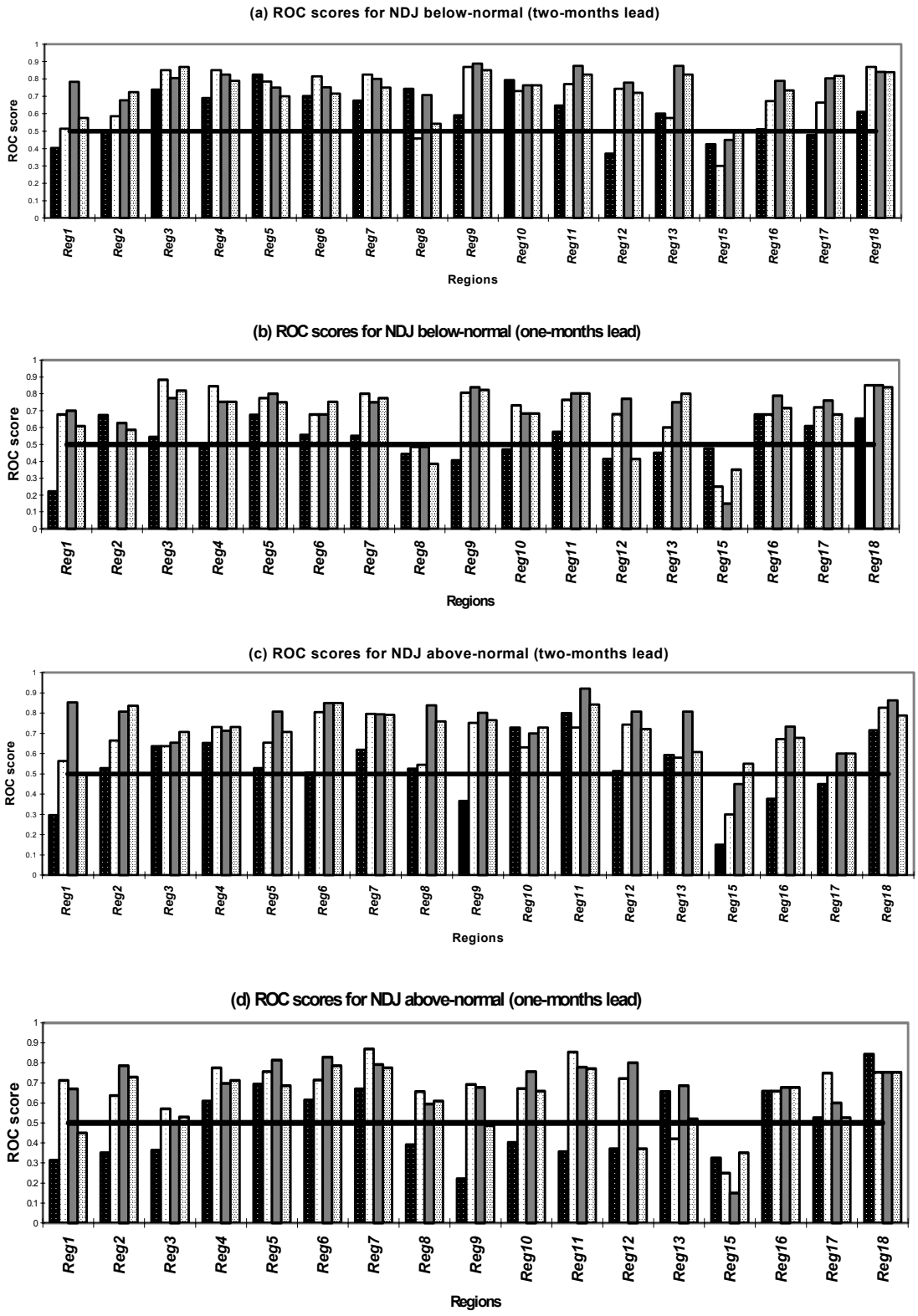


Figure 8. Same as Figure 6, but for the NDJ season.

### *3.3.3 December–January–February season*

A comparison of the models' skill for predicting DJF rainfall is shown in Figure 9. It is evident that the GCM rainfall forecasts continue to do a poor job relative to other forecasting techniques. At both lead-times, over most regions, the linear model and recalibration techniques clearly outperform the dynamical model. There are some noticeable differences between the skills of the recalibration methods and the CCA linear model, but in a few cases, the recalibration models are slightly outperformed by the simple statistical model, particularly at two-month lead-time. It is hardly surprising that the linear model shows highest skill during this season when tropical systems dominate the atmospheric circulation. The dominance of tropical circulation implies a more direct influence from regional changes in atmospheric heating such as those associated with ocean variability. This forced rainfall variability is more predictable than atmospheric internal variability, which is dominant during the early part of the season. Using a strategy of random guessing as reference (Figure 9 c,d), the raw-GCM ensembles continue to be the least performer, but attain positive scores over several regions particularly at one-month lead-time. The lowest overall scores are found over the Cape coast of South Africa (Region 1), and the northern part bordering the Democratic Republic of Congo (Region 15) where the forecasting techniques consistently show poor skills. The south-western coast of South Africa is mainly an austral winter rainfall region. A large part of Reg. 15 and its neighbourhood, fall within a bimodal rainfall regime with the peak rainfall received around October-December and March-May (Mutai et al. 1998; Indeje 2000). The apparent lack of skill in predicting austral summer rainfall over these regions is therefore not a major concern.

The ROC scores for probabilistic forecasts of below- and above-normal rainfall in each region are shown in Figure 10. Consistent with the results revealed by the RPSS, the ROC scores show that DJF rainfall over regions 1 and 15 are the least predictable, overall. The scores indicate that the CCA linear statistical model and the recalibration models appear to be able to predict both below- and above-normal DJF rainfall over much of the SADC region with some usable skill. This result is encouraging noting that it is accurate forecasts of extreme events that are of great value both practically and

economically. A minor difference in the scores of the PCR- and CCA-MOS models notwithstanding, there is no single model that performs much better than the other in predicting above- and below-normal rainfall.

### *3.3.4 January–February–March season*

The model predictions continue to show good predictability of rainfall over many areas during JFM (Figure 11). With climatology as reference strategy (Figs. 11a,b), the linear model and MOS models show an extensive coverage of positive scores. Negative scores are persistently found over much of Tanzania and the Cape region of South Africa, areas which are predominantly dry during this season. Despite the localised areas with low skill, the extensive coverage of positive skill suggests that the models adequately capture the overall structure of anomalous rainfall conditions. The skill of the GCM continues to be the lowest. Using a strategy of random guessing (Figs. 11 c,d), the skill of the models is positive across almost the entire SADC region, with highest skill over the central and southern regions.

The ROC scores for JFM, as shown in Figure 12, mirror the regions with highest predictability as indicated by the RPSS. However, the scores show a more positive picture indicating that even over regions with poorest predictability, the models can still simulate wet and dry conditions with some skill. For example, over Region 15, with the exception of the GCM, the models appear to simulate below-normal rainfall with some acceptable level of accuracy at one-month lead-time.

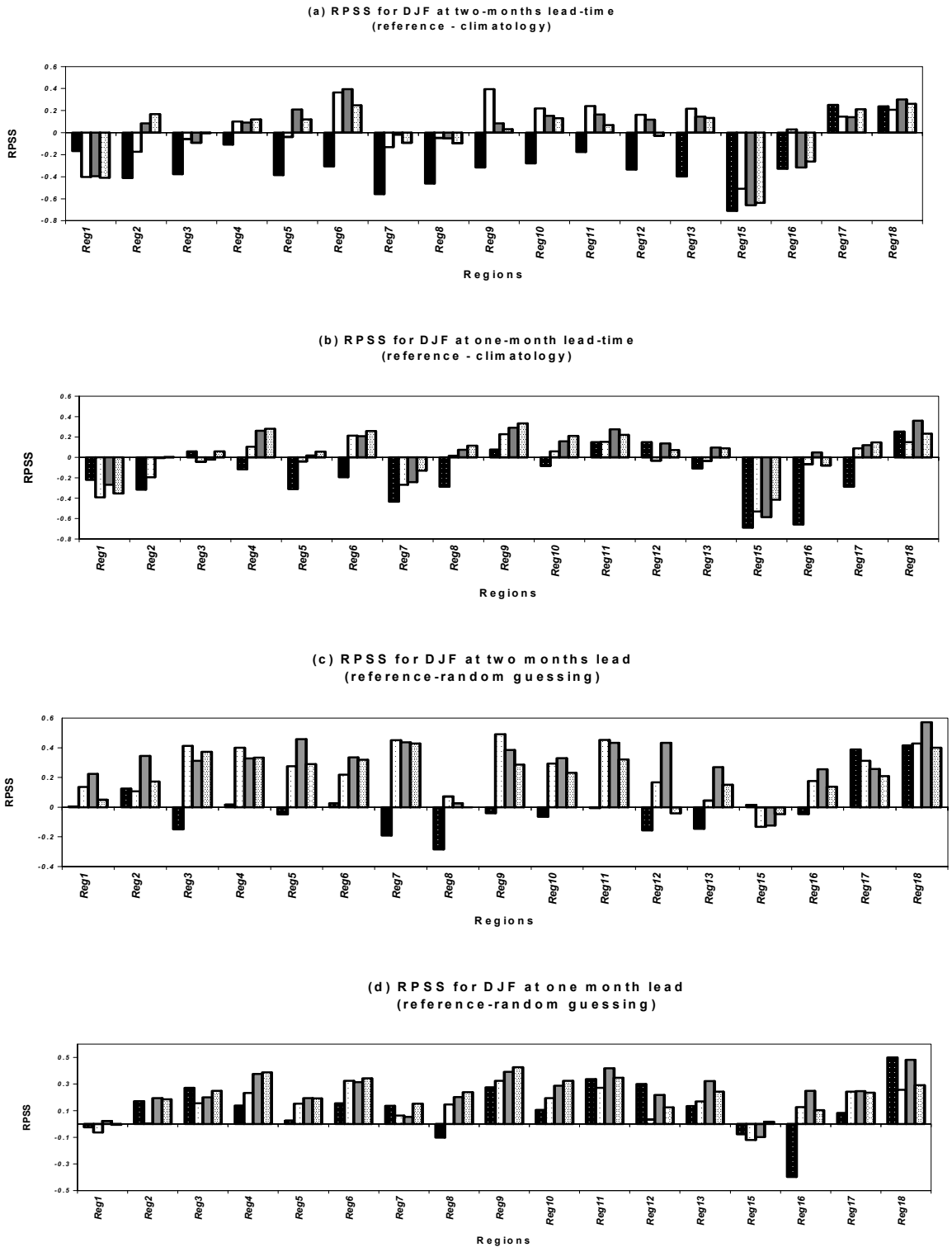


Figure 9. Same as Figure 5, but for the DJF season.

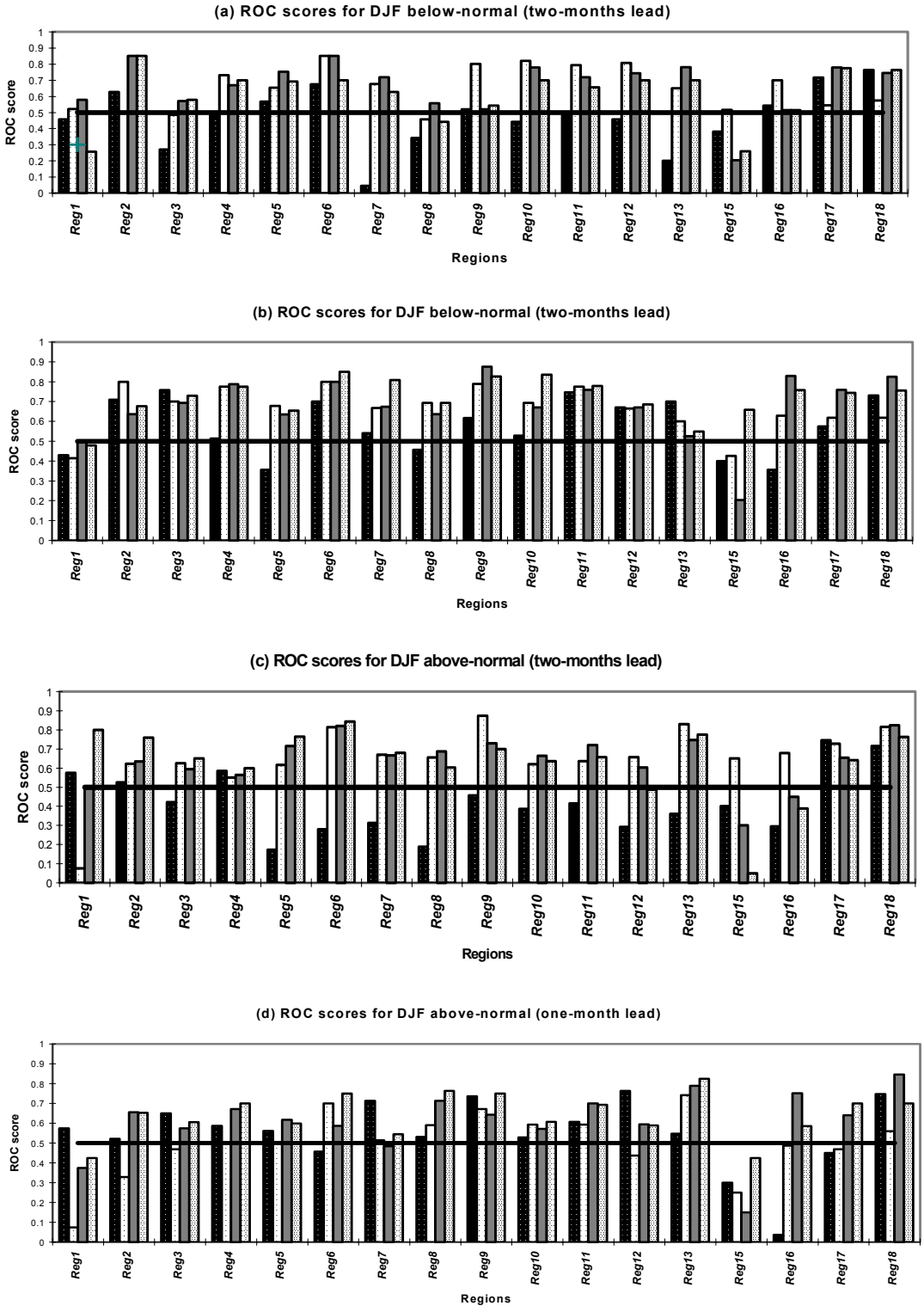


Figure 10. Same as Figure 6, but for the DJF season.

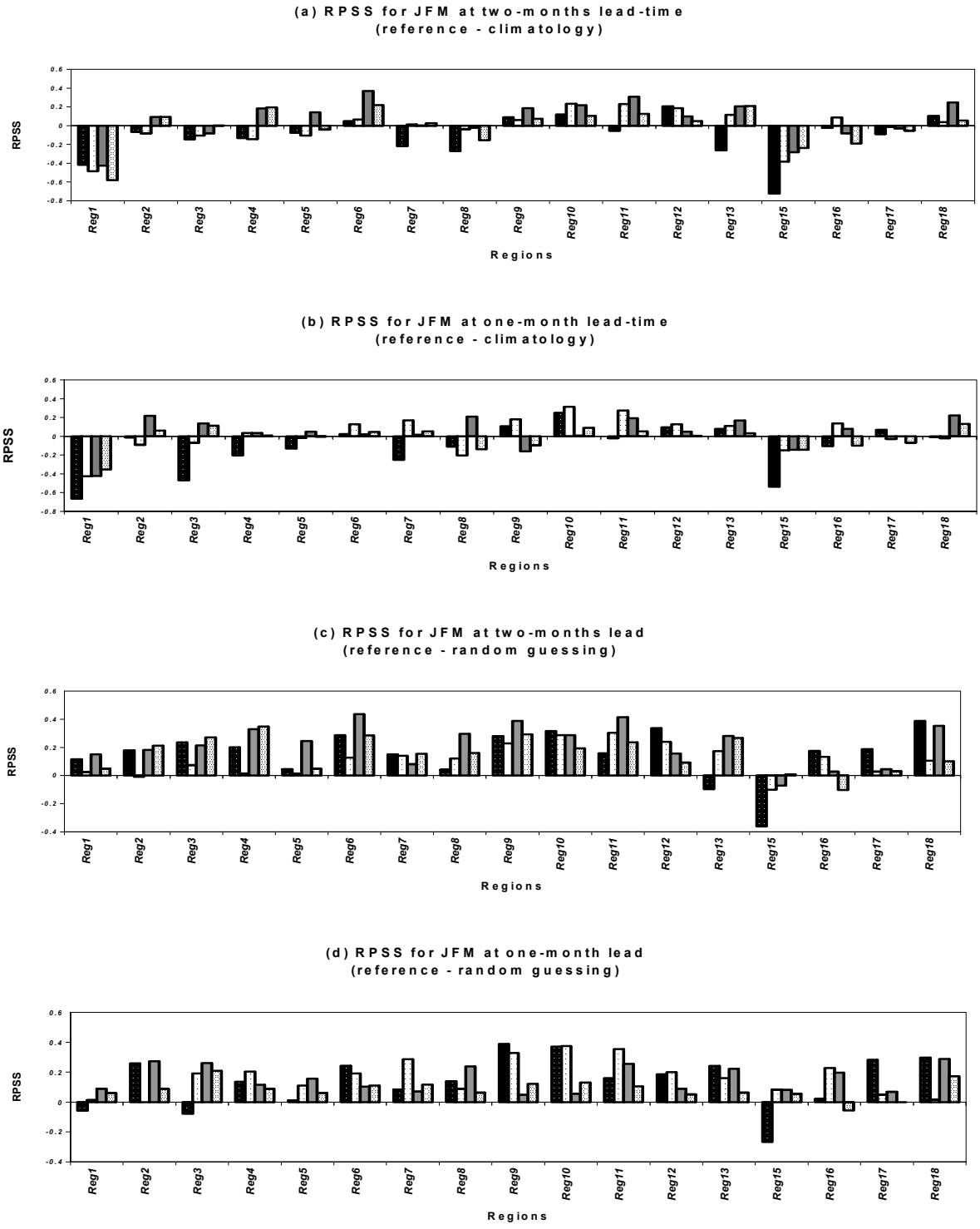


Figure 11. Same as Figure 5, but for the JFM season.

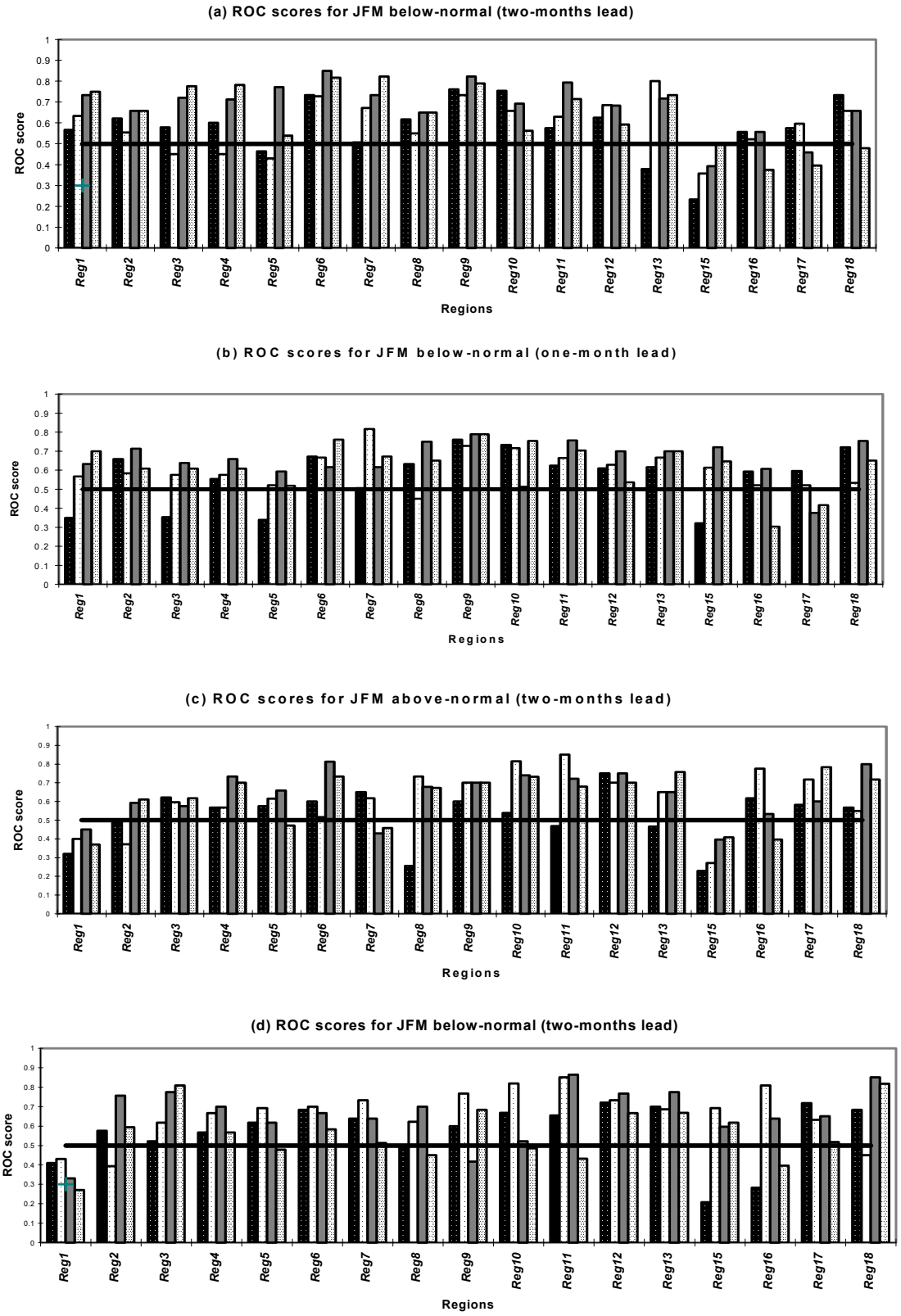


Figure 12. Same as Figure 6, but for the JFM season.

### *3.4 Seasonal dependence of skill*

A seasonal variation in predictability of austral summer rainfall over southern Africa has been has been observed elsewhere (e.g. Landman and Mason 1999b; Goddard et al. 2003). While the models appear to perform well in special cases and over specific regions, there may be some value in comparing their mean skill in a given season. This averaging provides a summary of the overall model performance during a given season. The RPSS based on the more competitive climatology reference strategy for each model have been averaged across the whole SADC region for a given season as shown in Figure 13. It is evident in the graph that on average, the PCR-MOS models perform better than its competitors. The CCA-MOS and the linear model show similar levels of skill with minor differences. The raw-GCM ensembles are the poorest performers.

It is apparent that the skill of the models is dependent on the season. Overall, OND is least predictable. During this season, the models forecasts are on average performing worse than the reference climatology forecasts at both lead-times. However, at one-month lead-time only the PCR-MOS model produces forecasts with skill exceeding that of the reference strategy throughout the austral summer period. Over much of the region, October is generally dry, which may contribute to the low skill in predicting OND rainfall. NDJ appear to have the highest forecast scores, particularly at two-month lead-time. The MOS models and the linear statistical model all outperform climatology during this season. At one-month lead-time the skill of the CCA-MOS model weakens. Model forecasts for DJF rainfall are more skilful at the shorter lead-time during which the MOS models beat climatology, but at one-month lead-time, the linear statistical model produces the most skilful DJF forecasts. It is the PCR-MOS JFM forecasts that are able to outscore the climatology forecasts at both lead-times. The improvement in forecast skill during the peak summer months is related to the dominance of tropical circulation whereby forced variability from direct heating such as that associated with SST variation exists.

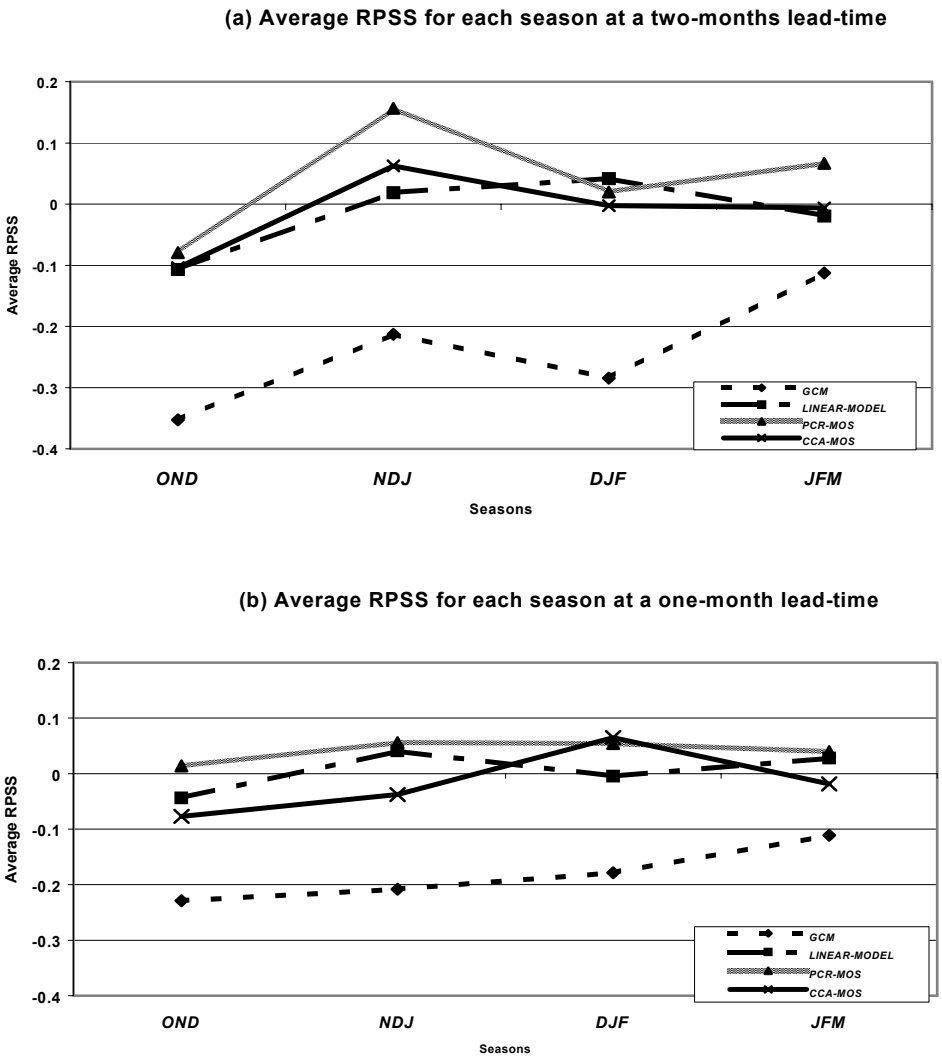


Figure 13. Area-average RPSS for the individual forecasting tools in a given season.

# 4.0 CHAPTER 4 POSSIBLE SOURCES OF PREDICTIVE SKILL

In this chapter, linear associations between regional rainfall and large-scale features of ocean variability, and the GCM large-scale circulation are investigated. The CCA spatial patterns and their corresponding temporal scores are used to diagnose possible physical mechanisms underlying the predictability of regional rainfall from large-scale features of the climate system. For brevity, only the first two pairs of canonical correlation patterns (exhibiting the highest canonical correlations, hence considered to be the most important) are presented in each case. The CCA patterns were computed for all the training periods of 28 (21), 31 (24), 34 (27), and 37 (30) years for the SST-rainfall (MOS) models to test their stability over time. By and large, there is a general similarity in the main features and because of this apparent robustness in predictor-predictand canonical patterns irrespective of the length of model-fitting period, only the analyses for the 34- (27-) year training periods will be presented in each case.

## *4.1 SST-rainfall link*

To draw inferences about the nature of ocean-atmosphere interaction responsible for the predictability of southern Africa rainfall from near-global SSTs, their (SSTs) space-time variability and the associated rainfall variations are investigated. In a broad sense, the predictor and predictand loading patterns at one- and two-month lead times are similar. This is related to the slow-evolving nature of SST patterns. For this reason, only the patterns obtained with the SSTs leading rainfall by two months will be presented here.

### *4.1.1 October–November–December season*

The spatial patterns of the first two canonical correlation analysis pairs linking SSTs and OND regional rainfall, and the associated time scores are shown in Figure 14. Areas where the predictor spatial loadings are statistically significant at the 5% level are shaded. The SST predictor pattern associated with the first CCA mode shows statistically significant negative loadings over much of the central equatorial Pacific Ocean covering the Niño 3.4 (170ºW–120ºW; 5ºS–5ºN) region, and positive loadings in the southwest Pacific and eastern tropical Indian Oceans (Fig. 14a). Negative loadings are also found along the western coast of North America. Associated with this predictor SST patterns

are positive loadings over the most skilfully predicted zones in the southeast, and negative loadings to the north and western zones (Fig. 14c). The correlation between the corresponding canonical vectors is 0.81 (Fig. 14e). Inspection of the SST predictor spatial patterns for mode 1 and the corresponding temporal scores suggest that this mode could be associated with interannual and longer-period (up to four years) modes of SST variability in the major oceans, notably in the tropical Pacific. ENSO in its developing stages during May–July (MJJ) may still play a role in this mode as evidenced by the larger loadings over the equatorial Pacific.

The SST predictor loadings for the second CCA mode are shown in Figure 14b. The pattern is dominated by statistically significant negative loadings over the tropical Indian Ocean and northern tropical Pacific Ocean. The correlation between the predictor and predictand canonical components time series for this mode is 0.67 (Fig. 14f). The temporal scores for this mode suggest that this mode could be associated with SST interdecadal variability and trends. The canonical component predictor time series show a prevalence of negative SST anomalies over the tropical Indian and Pacific Oceans during the decade extending through the 1970s and a positive trend from the early 1980s. Several authors discuss longer-period modes of SST variability in the major oceans, particularly the Pacific Ocean (e.g. Mantua et al. 1996; Gershunov and Barnett 1998). The canonical predictand map (Fig. 14d) suggests that the strongest response to the corresponding SST pattern is found over the southern parts of SADC, as indicated by the highest negative loadings. The results suggest that interdecadal oscillations in the major Oceans have notable impacts on the rainfall variability over the SADC region. These longer-period modes of SST variability may possibly modulate the effect of ENSO on regional rainfall, as is the case over western North America where the North Pacific Oscillation (NPO) has been found to modulate ENSO-related climate predictability (Gershunov and Barnett 1998).

Also present in this mode is a chain of SST anomalies of the opposite signs in the Southern Hemisphere mid-latitude oceans. Statistically significant positive loadings around New Zealand and southwest Atlantic Oceans are separated by significant loadings

of the opposite sign over the South Pacific Ocean. These broad areas of positive loadings correspond to the mean position of the midlatitude ridges whilst the negative loadings occur in preferred locations of low-pressure centres (south of Africa, southern Indian and Pacific Oceans) embedded within the circumpolar trough. Over and above the effect of interdecadal SST variability and trends the canonical predictor loading pattern for this mode could therefore suggest the presence of the Southern Hemisphere zonal wavenumber 3 (Chen and Yen 1997) signature on SADC rainfall fluctuations.

### *4.1.2 November–December-January season*

The loading patterns for the first canonical mode are shown in Figure 15a,c. The SST predictor patterns include statistically significant negative loadings in the equatorial and eastern Pacific and positive loadings over western Pacific. Positive loadings of a lesser magnitude are found over tropical Atlantic and eastern Indian Oceans indicating a lesser but significant contribution to forecast skill. As evidenced by the large and statistically significant loadings over the Pacific and the predictor canonical time series (see for instance years 1972, 1982, 1991-92 in Fig 15e), this mode represents a clear El Niño/La Niña signal on NDJ rainfall. The canonical correlation between the corresponding time series is 0.75 (Fig. 15e). Inspection of the predictor and predictand spatial patterns reveal that warmer (cooler) SSTs have often occurred in the equatorial Pacific Ocean from June–August during years characterised by below (above) average NDJ rainfall over homogeneous rainfall zones south of 15ºS and vice versa over the northern part and the coast of Angola. This result reflects a tendency for rainfall response to ENSO forcing in southern Africa to be opposite that of equatorial latitudes, which is in agreement with what has been found previously (e.g. Nicholson 1986; Ropelewski and Halpert 1987).

The canonical predictor map for the second mode (Fig.15b) features a tripole structure of loadings over the northern Pacific Ocean. Statistically significant negative loadings area also found over the north Indian Ocean extending to the Arabian Sea and the Bay of Bengal. Associated with these patterns are high positive predictand loadings over the northern SADC, suggesting that negative anomalies over the Arabian Sea and the Bay of Bengal could be somewhat related to wetter conditions over the north but these

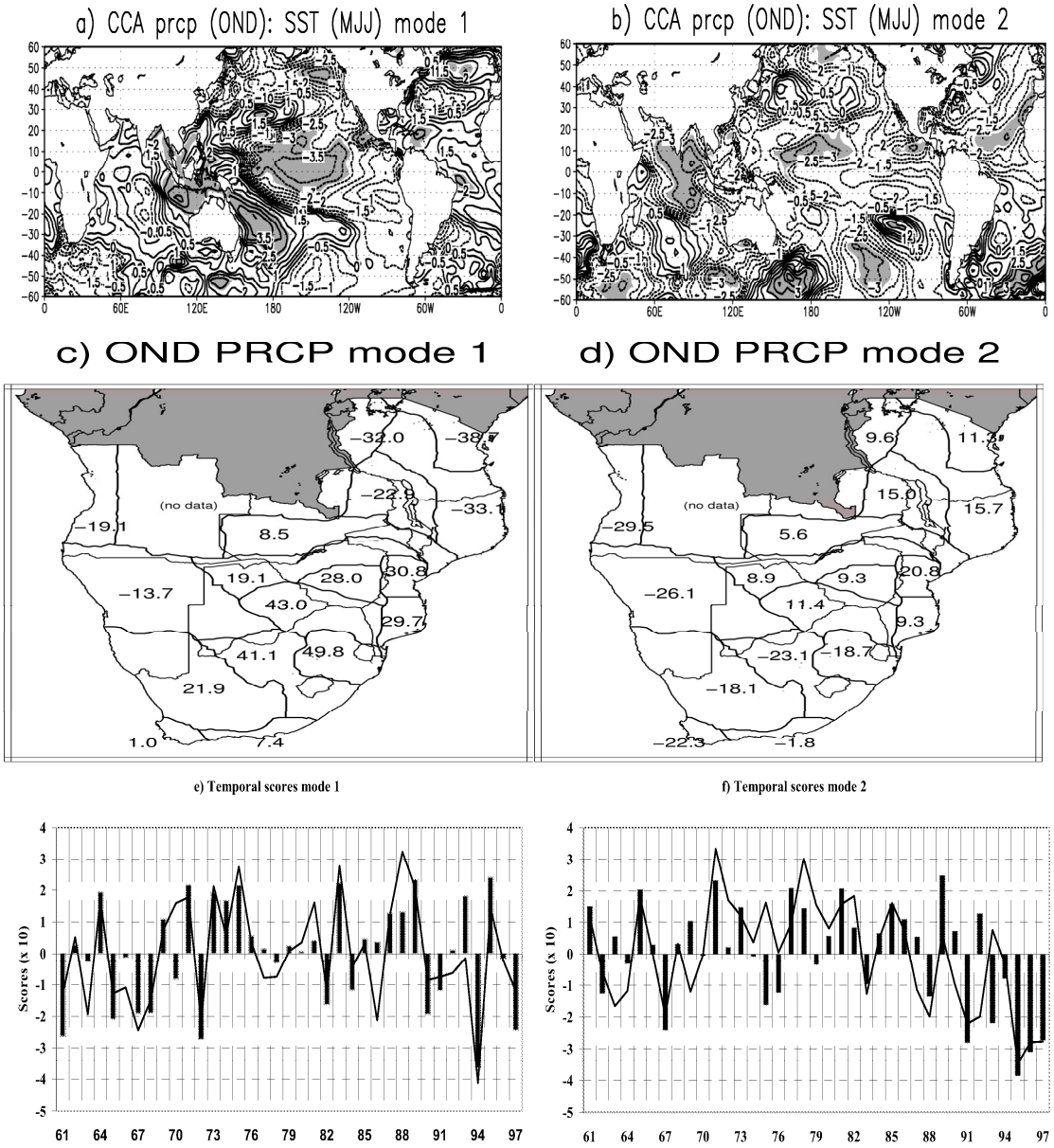


Figure 14. Canonical correlation maps and temporal scores for the first two CCA pairs of MJJ SSTs and OND rainfall. First (a) predictor and (c) predictand mode loading patterns. Areas whose loadings are statistically significant at the 5% level are shaded grey. (b) and (d) show similar patterns but for the second mode. The corresponding temporal scores of the SSTs (solid line) and precipitation (bars) are shown in (e) and (f) for mode l and mode 2 respectively.

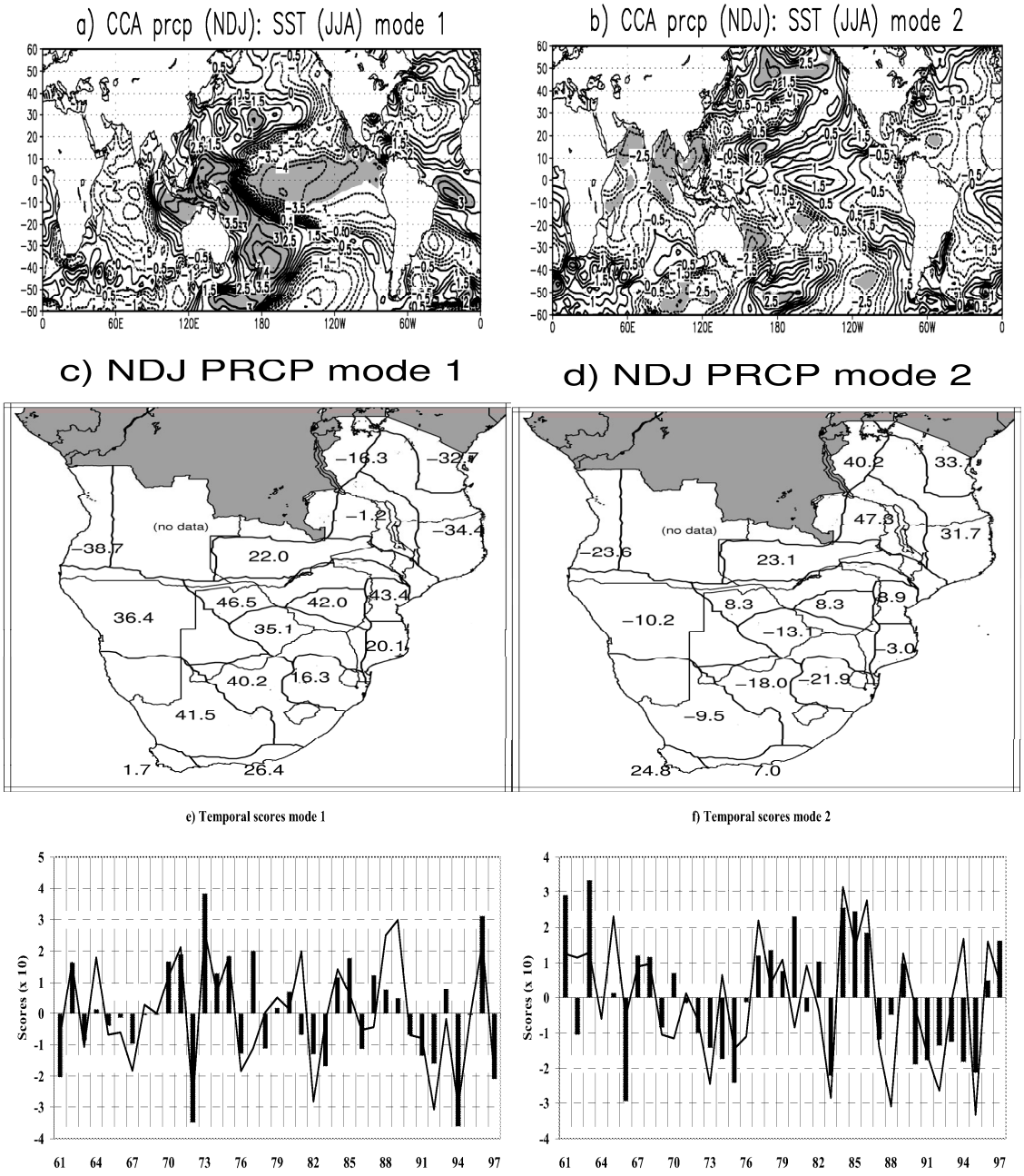


Figure 15. Same as Fig. 14 but for JJA SSTs and NDJ rainfall.

associations may not be of much interest over the seasonably dry northern areas during NDJ. The predictor loadings show a feature similar to the OND mode 2 pattern which show the presence of the Southern Hemisphere wavenumber 3 in the association with SADC rainfall. The correlation between the predictor and predictand canonical component time series for this mode is 0.59. The weaker predictand loadings (Fig. 15d) over the southern parts indicate that this mode plays a somewhat weaker role in comparison to ENSO influence.

### *4.1.3 December-January-February season*

CCA mode 1 describes the most significant source of predictability of DJF rainfall variability from sea-surface temperatures. The correlation coefficient between the two canonical component time series is 0.64 (Fig. 16e). The SST predictor loading patterns (Fig. 16a) for this mode suggest that most forecast skill comes from the tropical Pacific SST forcing. The spatial pattern includes strong negative loadings over much of the eastern tropical Pacific Ocean. Strong predictor loadings in the equatorial Pacific Ocean suggest the presence of the El-Niño/Southern Oscillation (ENSO) in the relationship with southern Africa DJF rainfall. The correlation between the SST 1961-97 time series for this mode and the Southern Oscillation Index is 0.41 (statistical significance at the 95% level). The DJF predictand loading pattern (Fig. 16c) shows mainly positive values over much of the southern regions (regions 2–12) and negative values over the northern part (regions 13– 18). Inspection of the predictor and predictand spatial patterns reveal that warmer (cooler) SSTs have often occurred in the equatorial Pacific Ocean from July–September during years characterised by below (above) average DJF rainfall over homogeneous rainfall zones south of about 15ºS and vice versa over the northern part.

Statistically significant loadings are also found over the equatorial Atlantic Ocean and the Mozambique Channel. While in the latter case, the statistically significant positive loadings are confined to a very narrow area, the feature is to be expected given that the southwest Indian Ocean and the Mozambique Channel SST anomalies exert a more direct influence on rainfall anomalies over southeastern SADC. According to the predictor and

predictand loading patterns, warmer SSTs over the Mozambique Channel and the Agulhas system are favourable of enhanced wetter conditions over nearby inland areas.

CCA mode 2 presents the second most important source of DJF rainfall predictability. The canonical correlation is 0.49. The canonical time series (Fig. 16f) suggest that this mode captures the influence of long-term trends or interdecadal mode of SST variability on DJF precipitation. The SST loading pattern (Fig. 16b) shows a broad area of positive loadings over the Pacific Ocean, with statistically significant contributions derived from the northern Pacific. Positive loadings are also found south of the African continent. Longer-period (interdecadal) oscillations in the major oceans, notably the Pacific have been widely discussed (e.g. Gershunov and Barnett 2003). From the 1960s to early 1970s there seems to have been have been a cooling trend in SSTs over much of the northern Pacific Ocean, followed by a reverse pattern from the mid 1970s onward. The predictand-loading pattern (Fig. 16d) suggests that mode 2 is associated with a dipole structure of DJF rainfall anomalies between the northern and southern parts of SADC. That is northern Pacific Ocean warming from the mid 1970s has been associated with diminishing DJF rainfall over the southern sector (an exception being the southern tip of South Africa), and vice versa to the north.

### *4.1.4 January-February-March season*

Figure 17a shows the first CCA pair between ASO predictor SSTs and JFM precipitation. The predictor patterns include positive loadings over the western equatorial Pacific, and the Northern and Southern Hemisphere midlatitude Pacific. Negative loadings are found over the southern subtropical Atlantic Ocean (Fig. 17a). The correlation between the corresponding canonical vectors is 0.7 (Fig. 17e). The SST loadings and canonical component predictor time series for this mode hint the presence of longer-period oscillations or trends in the SST-rainfall link. The predictand map for this mode (Fig. 17c) shows positive loadings over the north and extreme south and weaker negative loadings in regions 3-5 and 8. The non-uniform rainfall responses to large-scale forcing are still evident even during this season.

The predictor SST loadings for the second canonical mode (Fig. 17b) include positive loadings over the eastern tropical Pacific, the southwest Indian Ocean and the south Atlantic. Negative loadings appear over the southern Pacific and north Pacific off the western coast of North America. The predictand map for this mode (Fig. 17d) shows negative loadings over the southern and northern region, and positive over the central parts. The canonical correlation is 0.59 (Fig. 17f). Longer-term SST regimes are still evident in this mode.

### *4.2 GCM circulation field*

Over southern Africa, the weather observed during a particular season depends to a large extent on the mean low-, medium-, and upper-level atmospheric circulation as well as deviations from the mean state. Because of its geographical location, southern African weather is influenced by both tropical and extra-tropical circulation systems. Of particular importance to SADC weather are the semi-permanent subtropical anticyclones over the southeast Atlantic Ocean (St. Helena) and the southwest Indian Ocean (Mascarene), and transient continental low pressure systems that form during austral summer. Thus it is worthwhile to investigate the spatial pattern of the GCM low-level circulation as represented by the 850-hPa heights and link these patterns to the observed rainfall.

The statistical link between the GCM 850-hPa geopotential height and DJF rainfall over SADC will again be discussed based on the first two canonical patterns. There are some minor differences in canonical patterns at the two different lead times used in this research. However, in the interest of brevity only the patterns for MOS forecasts produced at a one-month lead, which have been generally found more skilful will be presented.

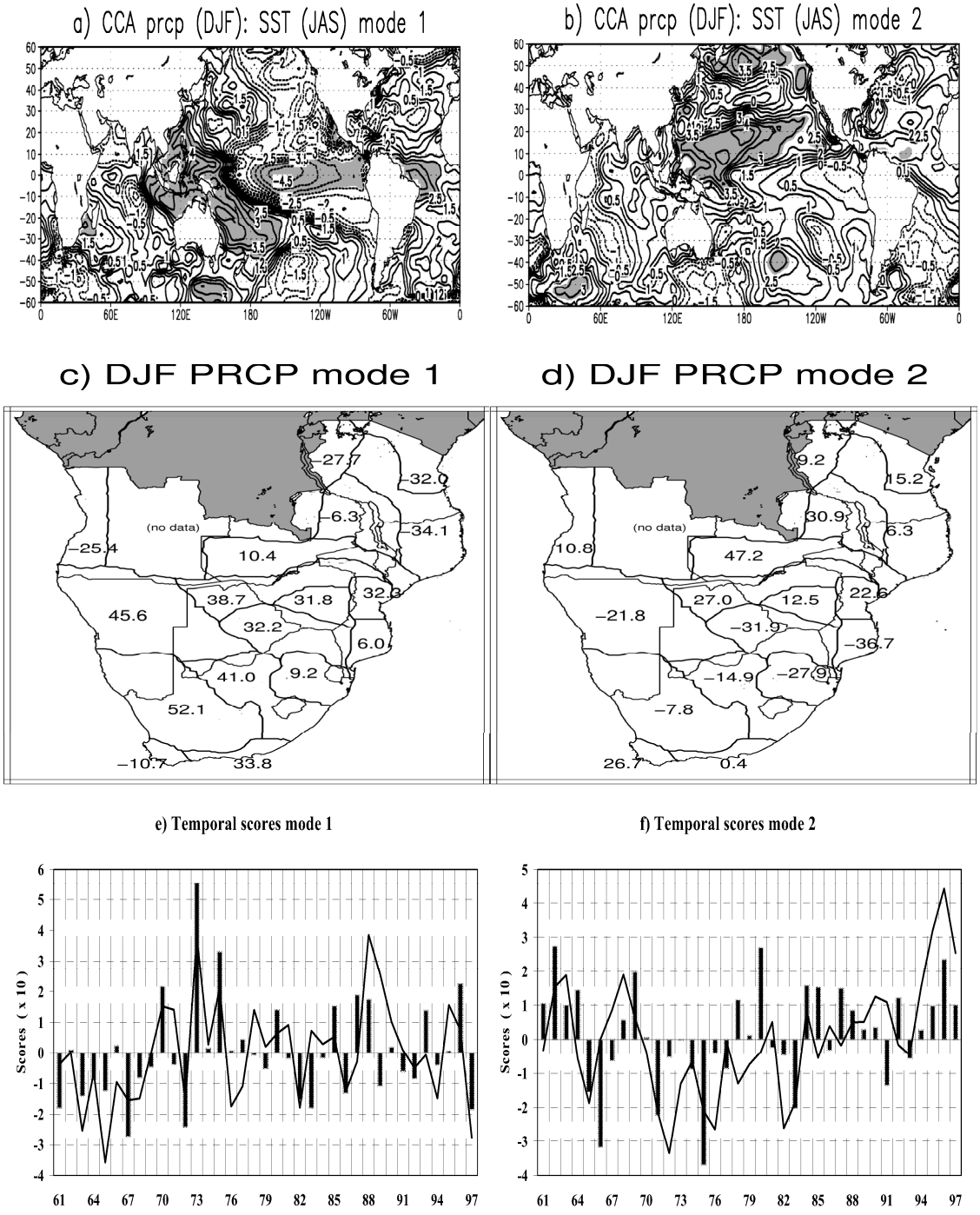


Figure 16. Same as Fig. 14 but for JAS SSTs and DJF rainfall.

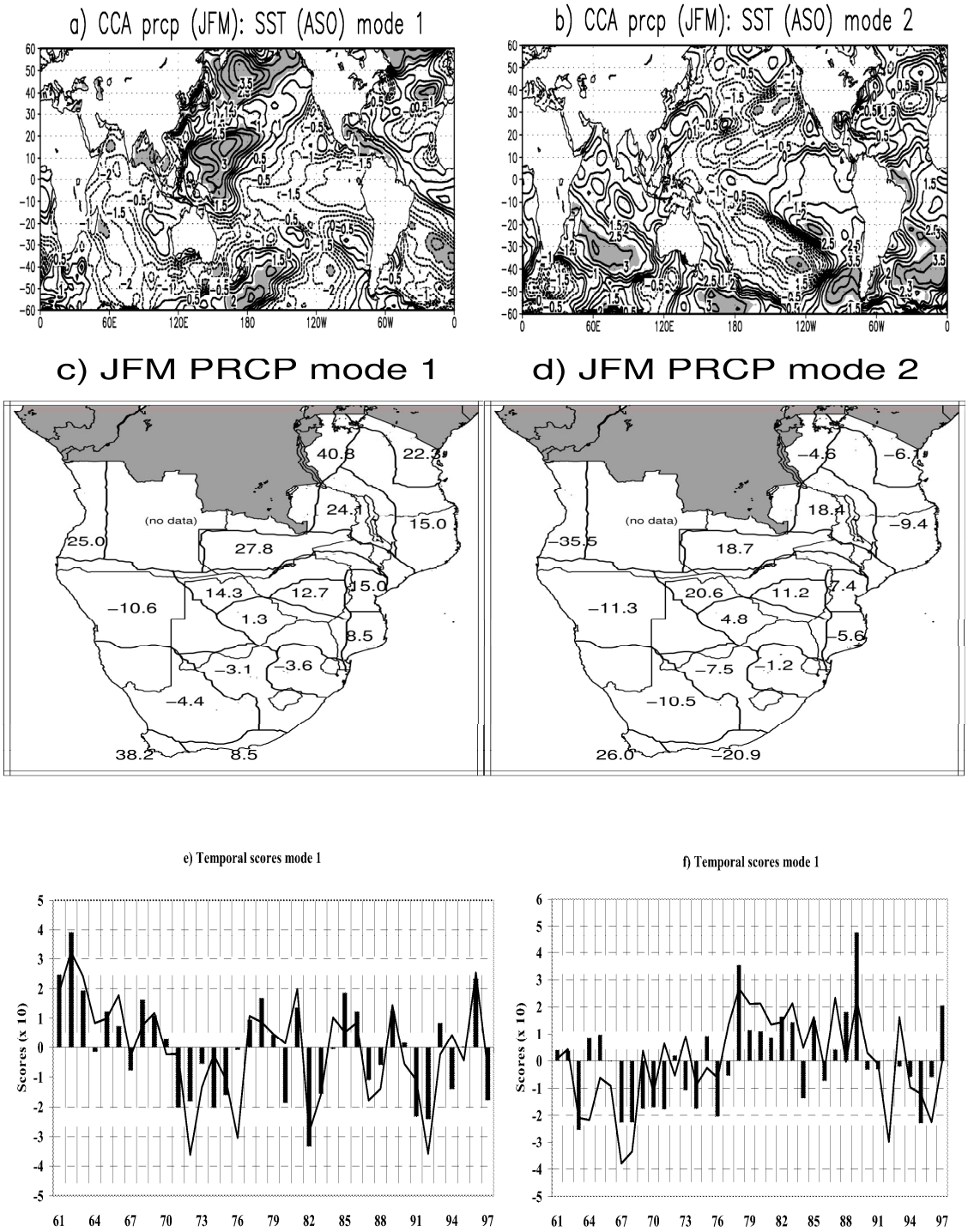


Figure 17. Same as Fig. 14 but for ASO SSTs and JFM rainfall.

### *4.2.1 October–November–December season*

The CCA diagnostic features for OND capture a physically meaningful link between regional precipitation variability and 850-hPa geopotential circulation. The first CCA pair, shown in Figs. 18a,c associates higher (lower) geopotential heights over much of the subcontinent and the bordering southeastern Atlantic Ocean with below- (above-) average OND rainfall over much of central and southern SADC. The predictor map also shows statistically significant positive loadings over the southwest Indian Ocean, southeast of Madagascar. The correlation between the respective canonical vectors is 0.64 (Fig. 18e). Lower geopotential heights over land areas at the lowest levels during this season could imply higher relative occurrence of continental low pressure systems favourable for ascending motion. Furthermore this feature could mean an "accelerated" southward migration of the ITCZ into the region resulting in an early onset of seasonal rains in the central areas (shown by higher positive loadings in Fig. 18c), a feature that could result in diminished rains in the northern parts (shown by higher negative loadings in Fig. 18c) which fall within the bimodal rainfall regime (refer to section 1.1) by shortening the short-rains season. Higher geopotential heights over the southwest Indian Ocean southeast of Madagascar are consistent with a more intense Mascarene anticyclone. One obvious influence of the strength of the southwest Indian Ocean on rainfall is related to moisture advection inland as will be discussed in the section below.

The second CCA pair (Fig. 18b,d; 0.41 correlation coefficient between the corresponding canonical vectors, Fig. 18f) associates lower (higher) 850hPa geopotential heights over the southeast Atlantic Ocean with anomalously dry (wet) conditions over the southern areas and vice versa over the central and northern parts. This pattern is quite reasonable from a physical point of view noting that a weaker southeast Atlantic (St. Helena) ridge is unfavourable for moisture laden low-level southeasterly winds from cold airmasses which typically follow the passage of frontal systems. The low-level southeasterly winds typical of circulation induced by an extension of the St. Helena anticyclone contribute a reasonable percentage of the rainfall received early in the season. The statistically significant negative predictor loadings over the area stretching from west into central Africa are probably related to enhanced rainfall over northern SADC from a deeper (or less diffuse) ITCZ.

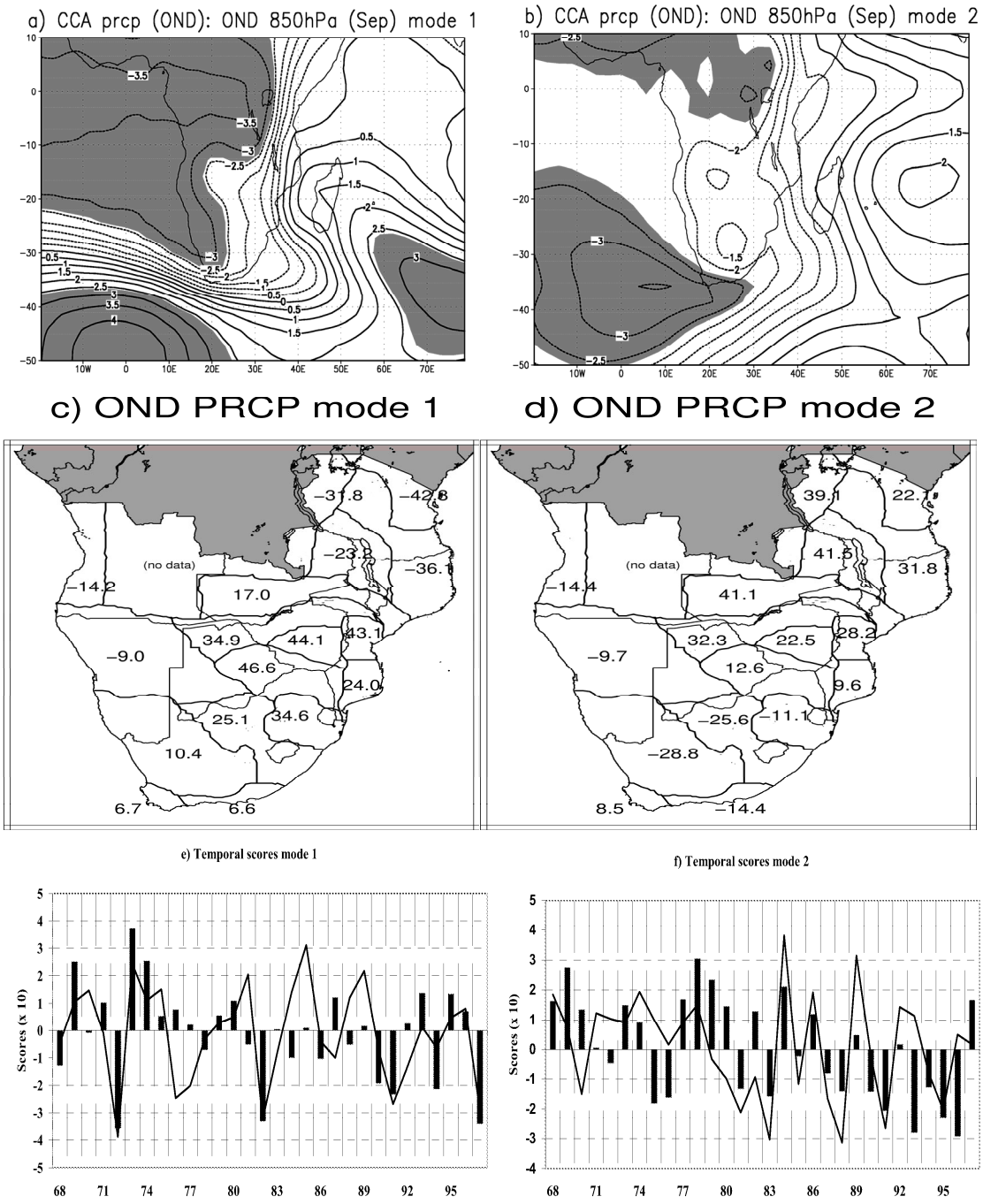


Figure 18. Canonical correlation maps and temporal scores for the first two CCA pairs of OND GCM 850-hPa geopotential height and OND rainfall. First (a) predictor and (b) predictand mode loading patterns. Areas where the predictor loadings are statistically significant at the 5% level are shaded in grey. (c) and (d) show similar patterns but for the second mode. The corresponding temporal scores of the 850-hPa geopotential heights (red line) and precipitation (green line) are shown in (e) and (f) for mode l and mode 2 respectively.

### *4.2.2 November–December-January season*

During this season, the first CCA pair (Figs. 19a, b) suggests that above- (below-) average precipitation over the central and southern parts of SADC goes along with a pronounced anticyclonic (cyclonic) pattern over the western Indian Ocean centred around Madagascar and an opposite pattern over the eastern Atlantic and the Congo basin. The correlation between the respective canonical vectors is 0.78 (Fig. 19e). The 'dipole' structure in GCM 850-hPa spatial pattern could be indicative of a wave nature of successive ridges and troughs/lows that exist in the atmosphere and have a significant effect on the weather/climate. The second CCA pair (Figs. 19 c,d) is similar to the OND first CCA pattern. The canonical correlation is 0.65 (Fig. 19f). This pattern, which is common for all the seasons, represents a meaningful physical relationship: increase (decrease) in low-level pressure (as represented by the 850-hPa geopotential height over high-elevation inland areas) tend to inhibit (aid) the occurrence of convection due to increases in subsidence (ascending motion), which results in diminished (enhanced) rainfall over the region.

The second CCA pair (Figs. 19 c,d) suggests that anomalous anticyclonic (cyclonic) flow over the southwest Indian Ocean centred east of Madagascar is favourable for enhanced rainfall over the central and northern parts (higher positive loadings in Fig. 19d). The canonical correlation is 0.65 (Fig. 19f). As shown by Rocha and Simmonds (1997a) this is a preferred location for anomalous cyclonic circulation in summer which has negative implications for SADC rainfall. The CCA pair for this mode suggest that the absence (presence) of this feature (anomalous cyclonic circulation) results in wetter (drier) conditions over the central and northern parts.

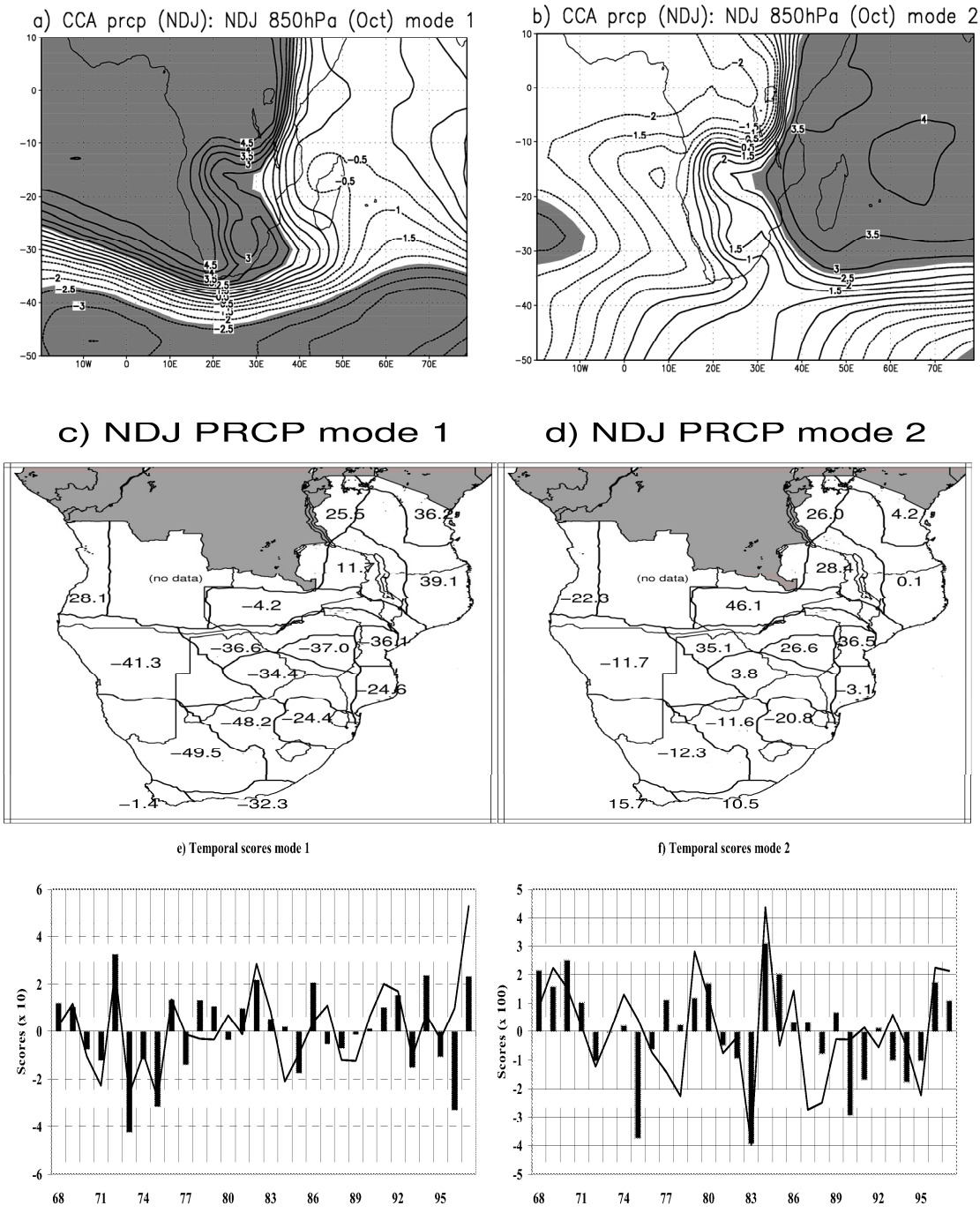


Figure 19. Same as Fig. 18 but for the NDJ GCM 850-hPa geopotential height and NDJ rainfall.

### *4.2.3 December-January-February season*

The first CCA pair, shown in Figs. 20a,c associates higher (lower) geopotential heights over much of the subcontinent and the bordering southeastern Atlantic Ocean with negative (positive) DJF rainfall anomalies over much of SADC. The correlation between the respective time series of these patterns is 0.79 (Fig. 20e). This pattern bears a lot of resemblance with the NDJ second CCA pair. The description of the plausible physical mechanisms responsible for the NDJ first CCA pair or the OND first pair should apply to the first DJF pair as well. The second canonical correlation pattern is shown in Figs. 20b,d. The correlation coefficient between the 850-hPa geopotential height and rainfall time series is 0.7 (Fig. 20f). This pair associates high (low) geopotential height over the southwestern Indian Ocean, south of Madagascar with positive (negative) DJF rainfall anomalies over much of the southern sector, and vice versa over the north. This pattern is quite reasonable physically in view of the fact that the southwestern Indian Ocean is a major source of moisture for precipitation formation over SADC. High (low) 850-hPa geopotential heights connotes an intense (weak) southwestern Indian Ocean (Mascarene) anticyclone, which may persist even up to the 700-hPa level, resulting in enhanced (weakened) advection of moisture inland. Sufficient (insufficient) moisture advection inland is consistent with enhanced (diminished) rainfall over the southern parts of SADC.

### *4.2.4 January-February-March season*

The first two CCA pairs for JFM are presented in Figure 21. The first CCA mode (canonical correlation 0.7; Fig. 21e) associates higher (lower) geopotential heights over the southwest Indian Ocean with below- (above-) average rainfall over central SADC and anomalies of the opposite sign over the southern and northern areas. This pattern shows the influence of the strengths of the subtropical anticyclones of DJF rainfall anomalies. During this season, tropical cyclones which form over the southwest Indian Ocean play a significant role in influencing rainfall anomalies. The presence of statistically significant negative loadings over the southwest Indian Ocean has some meaningful physical implications for the tracks of the tropical storms.

The spatial patterns for the second canonical mode (Figs. 21b,d) is quite similar to the first CCA pair for the other season. The canonical correlation is 0.56 (Fig. 21f). This

pattern appears in all season and the possible physical mechanisms it represents have been discussed.

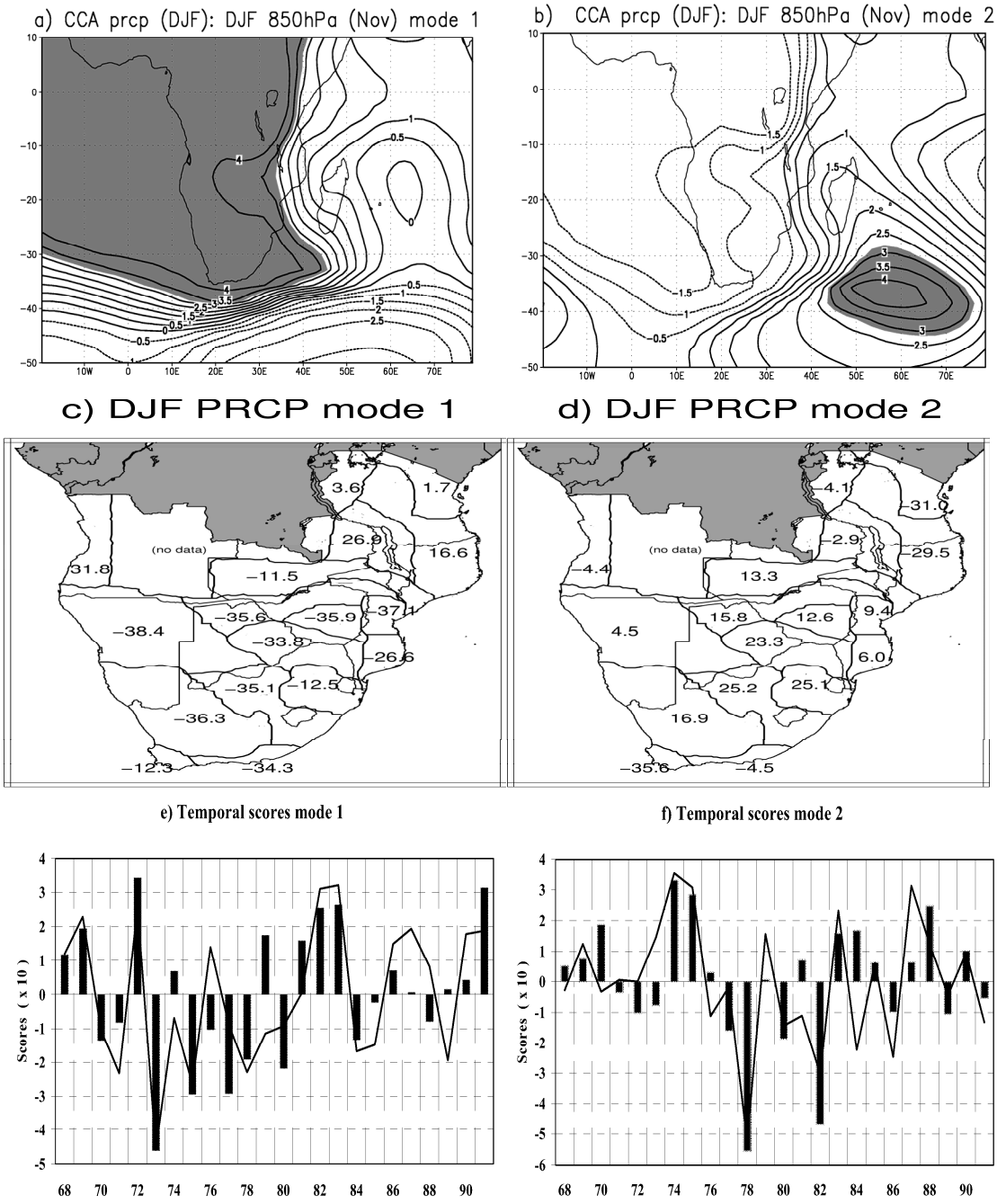


Figure 20. Same as Fig. 18 but for the DJF GCM 850-hPa geopotential height and DJF rainfall.

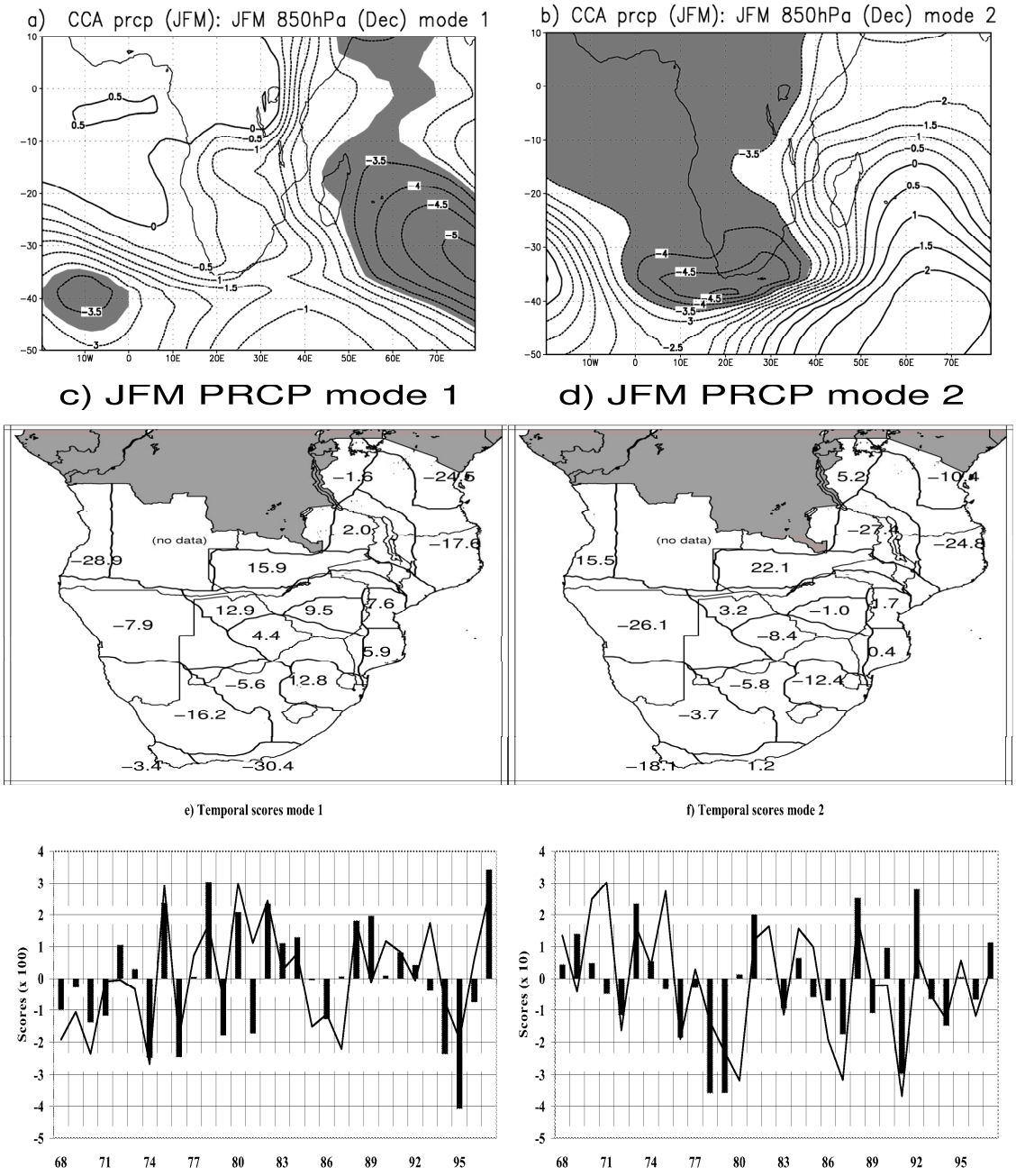


Figure 21. Same as Fig. 18 but for the JFM GCM 850hPa geopotential height and JFM rainfall.

# 5.0 CHAPTER 5 SUMMARY AND CONCLUSIONS

The main aim of this study was to get an idea of the skill of predicting summer rainfall over SADC using methods of differing complexities. Numerical models are the current state-of-the-art techniques used in seasonal climate prediction. The availability of the ECHAM4.5 GCM hindcasts enabled the assessment of the general skill of numerical models in predicting rainfall at regional scales over Africa south of the equator. The skill of a linear statistical model linking rainfall to near-global SSTs has also been evaluated. This was to answer the question of whether dynamical models have begun to outperform simpler empirical models. Efforts have been made to recalibrate the GCM hindcasts using statistical techniques and the extent to which the recalibration methods improve over the raw-GCM predictions has been assessed. Further, the performance of the recalibration techniques has been compared to get a general idea of which amongst them is best suitable for SADC summer rainfall prediction.

Disparate climate regimes exist within the Southern African Development Community (SADC). The complex surface features such as topography and their interaction with large-scale mechanisms induce notable heterogeneities in the seasonal rainfall distribution. Based on 255 rainfall stations across the region, 18 homogeneous rainfall regions have been identified from cluster analysis. These regions are believed to experience similar characteristics in terms of their seasonal to interannual rainfall variability. Of the 18 regions, some receive their maximum rainfall amounts outside the austral summer rainfall months. These include the austral winter rainfall region along the southwestern coast of South Africa (region 1; Fig. 4) and the bimodal rainfall regimes to the north (part of regions 15, 17, 18).

The results from this study reveal that successful austral summer rainfall forecasts can be made for much of the SADC region using the methods whose performance is assessed. Overall, highest forecast skill is confined to the southeastern parts of SADC. While the apparent spatial variation in skill may have resulted from higher signal-to-noise ratio over the southeastern areas where the station density is higher relative to the western parts, this result is essentially consistent with previous findings (e.g. Barnston et al. 1996; Landman

and Mason 1999b). Further, results from SST-rainfall relationships (e.g. Reason 1998, 2001) suggest the existence of stronger rainfall response to anomalous SSTs over the southeastern sector of the region implying higher potential rainfall predictability. Poorest forecast skill has been found over Region 1 and 15. In Region 15, anomalously dry conditions occurred more often (greater than 60 per cent) in all seasons during the testing period. The persistently low skill displayed in this region is reflective of the models' inability to predict the pervasive dryness, whose possible causes are beyond the scope of this study. Any lack of predictability of summer precipitation over these regions is however not a major concern because they receive their maximum rainfall outside the seasons whose predictability has been tested.

The results have shown that skill predicting seasonal precipitation varies as a function of the target season, with highest overall skill obtained during the peak summer months. Noting that the seasons overlap, having some months in common, the seasonal variation in skill is noticeable, albeit small. Overall, NDJ is predicted best followed by DJF, and then JFM, and OND is the least predictable season. Early in the rainy season (i.e. in October), higher rainfall amounts are received over the extreme parts of the region predominantly from extratropical systems. The generally lower skill during OND could be in part attributable to the predominantly baroclinic nature of the rain-bearing systems (van Heerden et al., 1988), which induce lower signal-to-noise ratios due to greater chaotic instability associated with them. However, during the peak austral summer months, when the ITCZ is in its southernmost position, tropical circulation dominates implying a more direct influence from local forcing mechanisms on the atmospheric circulation.

A linear statistical model linking near-global SSTs to regional rainfall has been developed and its skill assessed over a 12-year retroactive period 1989/90–2000/01. This model together with the raw-GCM ensembles has been used as a baseline reference against which the skill of the MOS models can be judged. The model demonstrates usable skill in predicting summer rainfall. The diagnostic features of CCA have been used to describe the form of association between the global SSTs and seasonal rainfall.

The results reveal that the Pacific Ocean is the most important contributor to the prediction skill during the peak austral summer months. The CCA predictand patterns exhibit a north-south structure with loadings of opposite signs over the region. This demonstrates that rainfall response to Pacific SST forcing is not uniform across the SADC region. The patterns show that in those years when southern SADC experiences anomalously dry (wet) conditions in response to Pacific SST forcing, anomalously wet (dry) conditions are often observed over the north. The ocean basins bordering southern Africa appear to be contributing least to the predictability of austral summer rainfall. This result may be misleading. SST fluctuations in the tropical Indian and Atlantic Oceans influence seasonal climate over SADC more significantly and directly than the Pacific. For instance, the southwest Indian and southeast Atlantic Oceans are the major source regions for maritime airmasses affecting the weather over the region. Even at seasonal and inter-annual time scales, there is evidence of the influence of the southeast Atlantic (Reason 1998) and subtropical south/southwest Indian Ocean on the circulation and rainfall patterns over southern Africa (Reason 1998, 1999, 2001, 2002). However, these two oceans are narrower compared to the broader Pacific Ocean. This is particularly true with the South Atlantic Ocean. Their significant contribution to climate variation notwithstanding, they are only represented in lower-order modes, which have not been shown here. Noting that they exert a direct influence on climate anomalies they could dominate simultaneous or shorter lead/lag SST-rainfall relationships. It is worth noting that ENSO-related SST variability in the Pacific encompasses the tropical oceans such that SST variations over the Indian and Atlantic are linked to ENSO (Nicholson 1997), with a time lag.

ENSO represent the most dominant mode in the ocean-atmosphere coupled system, which is highly significant later on in the rainy season. Consistent with findings by previous researchers (e.g. Ropelewski and Halpert 1987; Nicholson and Kim 1997; Mason and Goddard 2001), the results indicate an ENSO/rainfall dipole pattern over the southern and northern parts of the SADC region. During warm- (cold-) phase ENSO years, much of the southern parts, south of about 15ºS are prone to dryer- (wetter-) than-normal conditions particularly during the peak and late rainfall season, with the northern

parts experiencing anomalies of the opposite sign. The suppression of seasonal rainfall during DJF over much of southern SADC has had severe impacts on various climate-sensitive sectors of national economies, particularly on agriculture. The results from this study show that more predictability could be expected during extreme phases of ENSO. Advance guidance on the expected shift in the climate pattern in association with ENSO and other influential factors could be of great benefit. As evidenced by the rainfall response to the 1997/98 strong El Niño event, the magnitude, seasonal timing and duration, and consistency of ENSO forcing on regional climate vary with each event and are not necessarily determined by the strength of the event.

Over and above the influence of ENSO, rainfall anomalies are found to be influenced by trends and longer-term or interdecadal variations in the global SSTs. Again, the rainfall response to interdecadal variations in the SST patterns is not uniform across the region. This mode reveals that the global SST field has undergone significant changes during the past few decades, and this variability has had an effect on SADC austral summer rainfall. The results particularly suggest that partly in response to the apparent trend in global SSTs, for a significant portion of southern Africa, summer rainfall may have been diminishing since the mid-1970s. Analysis of austral summer precipitation trends over southern Africa during the period 1961–2000 (results not shown) have revealed that for much of the southern sector has been experiencing a rise in frequency of dry spells over the past two decades or so (i.e. the number of rainy days during summer has been reducing). However, the intensity of precipitation (defined by the ratio of total precipitation to the number of wet days) is increasing. But the net effect is an overall reduction in precipitation amounts over the bulk of southern SADC. These results are in agreement with Hewitson and Crane (2005) who noted an increase in the length of dry spells in South Africa using high-resolution gridded precipitation data sets. Using daily station data from eight of the countries whose data is used in the present study, New et al. (2005) noted a statistically significant increase in regionally averaged daily rainfall intensity and dry spell duration.

Climate models are sophisticated tools aimed at enhancing the understanding of the climate system (the atmosphere, biosphere, hydrosphere, cryosphere, geosphere, and their complex interactions) and to enable prediction of future climates. Owing to the complexity of these models and expenses required to run them in an operational environment, most national meteorological services within the region are incapable of running them. The availability of the ECHAM 4.5 GCM output, an atmospheric GCM, has prompted the investigation of its skill at a regional scale over southern Africa. This skill forms the baseline against which to judge recalibration techniques aimed at improving the model performance at smaller spatial scales over the region.

The raw-GCM ensembles have been proved to be the poorest performers at the spatial scales considered. This is a ubiquitous problem with low-resolution numerical models such as the ECHAM4.5 T42 GCM used here. Even the simpler linear statistical model outscores this complicated model, which attempts to accurately represent the physics of the climate system. The reasons for the poor performance of the GCM are not obvious. There could be a prevalent and serious error possibly related partly to coarse resolution resulting in inadequate representation of the earth's structure in the model and partly to parameterisation schemes used, amongst other possible sources of error. Joubert (1995) attributed the poor performance of coarse resolution GCMs in simulating rainfall totals over central southern Africa, where rainfall is predominantly convective, to simplistic parameterisation of convective processes. At the shortest lead-time (one-month) the model skill improves but it still performs poorer than the other models. This suggests that information from the GCM at shorter lead times may still provide useful ancillary information, if regarded with caution. The results have indicated that although there seem to be a systematic error in simulating grid-point rainfall totals, the model is not completely unreliable. This study has shown that recalibrating the model forecasts offers an improvement to skill and provides more useful climate information.

The ECHAM 4.5 GCM-output/rainfall relationship is in agreement with Landman and Goddard (2002), in which the 850-hPa geopotential height from an earlier version of the same model (EHCAM 3.6) was found to be the most skilful predictor of southern Africa

austral summer rainfall. Much of inland SADC has an altitude greater than 1000 m above mean-sea-level. The 850-hPa geopotential therefore gives a good representation of the low-level circulation. Empirical relationships between archived records of the GCM 850-hPa geopotential height have been derived using two regression-based techniques. These model output statistics (MOS) models are based on principal components regression (PCR) and canonical correlation analysis (CCA). These statistical methods are being used to derive empirical relationships among GCM simulated fields and regional rainfall, which is later, applied in seasonal climate prediction. However they are unable to accommodate non-linear relationships, which inherently exist among climate parameters. Therefore, the inherent advantage of applying these methods in recalibrating GCM output is that complex non-linear relationships among climate variables, which they cannot accommodate alone, are incorporated in the GCM simulations. When applying these methods in statistical model recalibration, we make some assumptions, which are mentioned by Wilby and Wigley (2000). We assume that (i) there is a strong link between grid- and marco-scale versus grid- and sub-grid-scale predictor variables; (ii) future changes of the large-scale variables are small so that the derived empirical relationships are valid in the future; (iii) the large-scale variables acting as predictors in the MOS models and their possible future changes are adequately well simulated by the GCM.

The models have been tested over a 12-year retroactive period and their skill evaluated quantitatively. We selected the 1989/90–2000/01 period for testing model performance with the belief that all the variables used (both predictor and predictand) would have sufficient opportunity to span their naturally expected range. The MOS models outperform the low-skill raw-GCM ensembles but only slightly outscored the CCA linear model. PCR-MOS appears to do a slightly better job than its competitors. This is encouraging given that the PCR procedure is technically less complex than CCA. The fact that there is no huge difference in the MOS models' skill could be because in a broad sense, PCR and CCA perform the same task: they use linear regression to relate historical predictor and predictand data. They only differ in procedure.

During the early 1990s, partly in relation to ENSO, the rainfall pattern particularly over the southeastern parts showed a tendency toward dryness, which has been skilfully predicted by the models. The models' ability to predict anomalously dry events is encouraging. Of the reported natural disasters within the SADC region, those related to weather/climate dominated. Droughts have occurred recurrently over the region resulting in severe deficiencies in soil moisture hence failure in agricultural production. The severe effects of droughts are often prolonged. Guidance in advance regarding a likely shift in the seasonal rainfall pattern, such as expected rainfall suppression in the region would therefore be very important for planning purposes in the agricultural industry and other socio-economic activities in the region.

The ultimate goal of the climate community worldwide is to provide more skilful and reliable climate forecasts at spatial and temporal scales consistent with what is generally required by the climate information users. This research is a step in that direction. It is now widely accepted that because of the spatial resolution of most GCMs, the reliability of GCM output variables (e.g. precipitation), which critically depend on sub-grid-scale processes and parameterisation schemes used is low. As such the raw-GCM precipitation forecasts are frequently considered as nothing more than a guide as to how the next seasons' climate is likely to shift given the prescribed boundary forcing in each case. An encouraging result of this study is that the efforts to improve GCM simulations using the two statistical methods proved fruitful. It is clear from the results that coarse resolution GCM forecasts can be made more useful at regional or smaller scale through some form of post-processing to correct for model biases. Statistical downscaling in simpler and cheaper relative to dynamical downscaling but provide huge improvements in model performance. The use of statistical recalibration methods is recommended. PCR-MOS and CCA-MOS have demonstrated almost comparable skill levels. Use of either method, but not necessarily both is recommended. CCA linear model is not clearly inferior to the MOS models. The continued use of linear statistical models parallel with more sophisticated climate forecasting methods is highly recommended.

Having assessed the performance of different forecasting techniques, some suggestions for future work would include:

- An improvement in the data quality over the western parts of the SADC region would enable a fair judgement of the spatial variation in predictive skill, particularly forecasts made from empirical models. Although previous studies have shown weaker teleconnections over these regions, but this may be in part attributable to the poorer data quality relative to the eastern parts.
- An assessment based on multiple GCMs tested over a reasonably longer period would provide more robust conclusions on their general performance in predicting rainfall at smaller spatial scales in southern Africa. This would further enable comparisons between skill of individual GCMs and their weighted combination based on past performance, or any other criterion.
- There is need for assessing the extent to which a combination of dynamical and statistical downscaling can offer improvements on the deficiencies of raw GCM forecasts. This would entail nesting a regional climate model (RCM) within a GCM and then applying statistical post-processing to the RCM output.
- This study has focussed on predictability of rainfall in the upper and lower terciles. There is an urgent need to look at more extreme events such as rainfall in the upper or lower $5^{th}$ percentile